

---

# ENHANCING FOUNDATION MODELS FOR TIME SERIES FORECASTING VIA WAVELET-BASED TOKENIZATION

**Anonymous authors**

Paper under double-blind review

## ABSTRACT

There is a major open question about how to best develop foundation models for time series forecasting. *Tokenization* is a crucial consideration in this effort: what is an effective discrete vocabulary for a real-valued sequential input? To address this question, we develop WaveToken, a wavelet-based tokenizer that allows models to learn complex representations directly in the space of time-localized frequencies. Our method first scales and decomposes the input time series, then thresholds and quantizes the wavelet coefficients, and finally pre-trains an autoregressive model to forecast coefficients for the horizon window. By decomposing coarse and fine structures in the inputs, wavelets provide an eloquent and compact language for time series forecasting that simplifies learning. Empirical results on a comprehensive benchmark, including 42 datasets for both in-domain and zero-shot settings, show that WaveToken: *i*) provides better accuracy than recently proposed foundation models for forecasting while using a much smaller vocabulary (1024 tokens), and performs on par or better than modern deep learning models *trained specifically on each dataset*; and *ii*) exhibits superior generalization capabilities, achieving the *best average rank across all datasets* for three complementary metrics. In addition, we show that our method can easily capture complex temporal patterns of practical relevance that are challenging for other recent pre-trained models, including trends, sparse spikes, and non-stationary time series with varying frequencies evolving over time.

## 1 INTRODUCTION

Time series forecasting is integral to decision-making processes in many domains, including finance, healthcare, supply chain optimization, and climate science. Over the last decade, the field has seen a gradual but steady adoption of “global” deep learning models in lieu of traditional “local” statistical models (Lara-Benítez et al., 2021; Benidis et al., 2022). Recently, the success of large language models (LLMs) on natural language and vision applications has spurred an increasing interest for developing similar “foundation models” in other fields (for example, Subramanian et al. (2024); Golling et al. (2024); Ansari et al. (2024); Das et al. (2023)). These efforts aim at building general-purpose machines able to learn complex representations from vast amounts of data and to generalize to a wide variety of tasks, based on the premise that LLMs are general pattern recognizers (Mirchandani et al., 2023). In other words, if a problem can be reduced to that of modeling an arbitrary sequence of tokens defined on a discrete vocabulary, then an autoregressive transformer might be capable of learning non-trivial relationships via next-token prediction, regardless of the inputs representing text or not. The sequential nature of time series forecasting aligns seamlessly with this perspective, which is why several recent works have proposed adapting transformer-based architectures into foundation models for time series (see Section 2 for a review).

Tokenization is a crucial albeit still understudied (Dagan et al., 2024) component of LLMs, as it provides the vocabulary on which token streams are defined and the autoregressive structure is learned. While in principle transformers can learn arbitrary dependencies, in practice it matters whether the architecture can efficiently leverage specific structures in the inputs. In the context of time series forecasting, it is then important to answer the following question: what is the most appropriate *discrete* vocabulary for a *continuous* (real-valued) sequential input? In other words, what is the correct “language” for time series forecasting? As the goal is to develop a unified model with excellent forecasting performance on unseen datasets, an ideal dictionary of tokens should be as expressive as possible while also being compact, in order to efficiently represent the extremely high variety of non-

054  
055  
056  
057  
058  
059  
060  
061  
062  
063  
064  
065  
066  
067  
068  
069  
070  
071  
072  
073  
074  
075  
076  
077  
078  
079  
080  
081  
082  
083  
084  
085  
086  
087  
088  
089  
090  
091  
092  
093  
094  
095  
096  
097  
098  
099  
100  
101  
102  
103  
104  
105  
106  
107

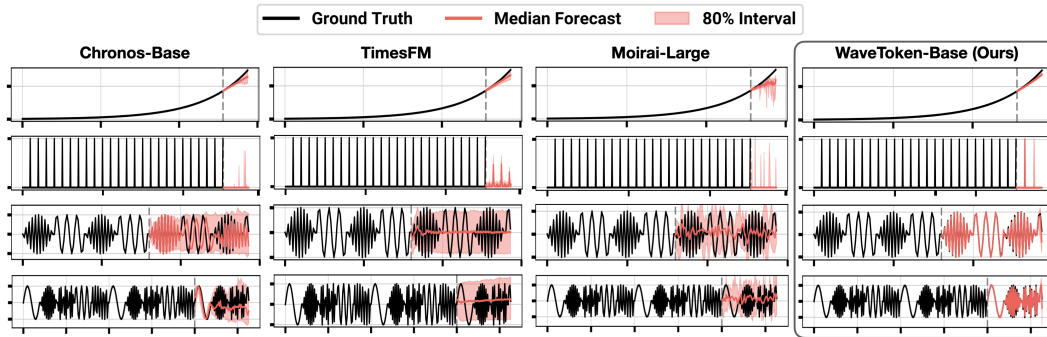


Figure 1: **WaveToken-Base (199M parameters) provides excellent forecasts with very low uncertainty.** Performance of different foundation models for time series forecasting on complex patterns of practical relevance: Chronos-Base (201M), TimesFM (200M) and Moirai-Large (311M) struggle to capture exponential trends (*top row*), sparse spikes (*second row*), and non-stationary signals with 2 and 5 frequencies evolving over time (*bottom two rows*).

stationary real-world time series. In addition, different “languages” can exhibit various dependency structures: although time series have a natural “order” dictated by time, one might ask whether there exists a mapping providing a more eloquent re-ordering in a suitable space that exposes important features and simplifies learning. Popular existing frameworks leverage temporal patches (e.g., Das et al. (2023)) or quantization into prescribed bins (e.g., (Ansari et al., 2024)) and lead to competitive performance in standard settings. However, by preserving the natural temporal dependency in the input, these approaches tend to focus more either on the recent history or uniformly over all time steps. As a result, they struggle to simultaneously capture both local and global patterns that often represent relevant cases in practical applications (see, e.g., Figure 1).

**Main contributions.** In this work, we propose and analyze a tokenizer based on wavelets, which are families of basis functions used to decompose a signal into small waves with high resolution in both time and frequency domain (Mallat, 2009). In particular, we develop a tailored pre- and post-processing tokenization pipeline — WaveToken — that allows the model to learn directly in the space of sparse wavelet coefficients. This yields a compressed but highly expressive vocabulary that facilitates the encoding of complex non-stationary time series. In addition, it provides an explicit multi-scale structure in the inputs, which the model learns to exploit by effectively forecasting from coarser to finer resolutions. We pair our wavelet-based tokenizer with the popular T5 encoder-decoder architecture of Raffel et al. (2020) and pre-train it on a large corpus of time series from different domains. We evaluate WaveToken on a comprehensive in-domain and zero-shot benchmark made of 42 real-world datasets and compare it with traditional statistical models, recent LLM-based forecasters, and state-of-the-art deep learning models. Empirical results show that

- i*) in terms of **accuracy**, WaveToken achieves superior forecasting performance and always performs on-par or better than all other baselines with respect to three complementary metrics, while using a *much smaller vocabulary* (1024 tokens) than recent foundation models for time series.
- ii*) WaveToken exhibits superior **generalization** capabilities, achieving the *best average rank across all datasets* for all metrics. In addition, our method can easily capture complex temporal patterns in several edge cases relevant for practical applications, such as exponential trends, sparse spikes and signals with different frequencies varying over time, as shown in Figure 1.

Overall, our findings not only suggest that wavelet-based tokenization can provide a compelling language for time series forecasting with LLMs, but also position our approach as a promising avenue for developing general-purpose, information-efficient forecasting models.

## 2 RELATED WORK

**Tokenization in LLMs.** Most tokenizers originate from the natural language processing (NLP) literature and have been developed and studied for various domains such as math (Singh & Strouse,

2024), code (Zheng et al., 2023), and several languages (e.g., Tolmachev et al. (2018); Alyafeai et al. (2023)). In modern LLMs, the most popular tokenizers learn a dictionary directly on data, such as variants of Byte-Pair Encoding (BPE; Gage (1994)). Tokenization of real-valued numbers has received particular attention due to the difficulty of finding what is the most appropriate discrete vocabulary for a continuous input. One of the most popular methods is training a Vector Quantized-Variational AutoEncoder (VQ-VAE) (Van Den Oord et al., 2017), which learns a dictionary of  $k$ -dimensional codewords to capture latent representations. Instead of learning a token for each numerical value, Golkar et al. (2023) proposes a fixed scheme that allocates a dedicated embedding vector for numerics and scales it by the number value, thereby improving efficiency and generalization. In this work, we similarly adopt a fixed scheme, but employ a tailored wavelet decomposition that enhances the crucial spectral properties of time series signals.

**Wavelet-based forecasters.** Several approaches have tried to embed wavelets in forecasting pipelines. An early example is that of Papadimitriou et al. (2003), who integrate the discrete wavelet transform with ARIMA modeling to capture complex patterns over long time periods. More recently, Zhou et al. (2022) proposed to substitute attention blocks with Fourier- and wavelet-enhanced blocks in the transformer architecture. Within this line of work, Zhang et al. (2022) proposed to model trend and seasonality separately with an MLP and Fourier attention, respectively. In addition, they showed that under *linear* transformations, attention models in time domain, Fourier domain and wavelet domain have the same representation power. Sasal et al. (2022) leverage a redundant wavelet transform that yields  $J$  series of coefficients (one per decomposition level), each having the same length as the original time series. They then learn a separate transformer model for each scale. To the best of our knowledge, WaveToken is the first application of a maximally decimated wavelet transform to build a tokenizer tailored for time series forecasting with LLMs.

**Modeling and generation of signals.** Different methods in the signal processing literature propose to integrate spectral or wavelet decomposition with deep learning architectures to enhance the capabilities of these models on a variety of tasks. Apart from the already-mentioned VQ-VAE (Van Den Oord et al., 2017), several works exploit spectrograms and log-mel spectra, for example, as pre-processing steps on medical or audio data (Choi et al., 2023; Purwins et al., 2019). Similarly, audio codecs (Zeghidour et al., 2021) are emerging as a critical technique to bridge the gap between continuous waveforms and token-based language models. As for image generation, Guth et al. (2022) proposed to speed up denoising by learning diffusion models in the wavelets domain. Recent concurrent works by Tian et al. (2024), Mattar et al. (2024) and Zhu & Soricut (2024), learn an autoregressive model on a multi-scale sequence or in the space of 2D wavelet coefficients.

**Foundation models for time series forecasting.** Several approaches are being developed to adapt LLMs to other domains, such as time series forecasting. Recent efforts in this direction include, e.g., Xue & Salim (2023), which converts time series into text and re-frames the task as a question-answering problem; Gruver et al. (2024), which tokenizes real-valued data as strings of digits and leverages models such as GPT-3 (Brown, 2020) and Llama 2 (Touvron et al., 2023); and Jin et al. (2023), which prompts a frozen LLM with a prefix describing the task and patch embeddings of time series aligned with text prototypes. Recently, Rasul et al. (2023); Goswami et al. (2024); Das et al. (2023); Ansari et al. (2024); Woo et al. (2024); Talukder et al. (2024) proposed different paradigms to pre-train transformer-based architectures on a large corpus of time series. See also Zhang et al. (2024) for a recent survey. While these works adopt domain-specific designs such as patching, lags and time features, none of them tackles the problem by learning an autoregressive model in the expressive space of time-localized frequencies.

### 3 LANGUAGE MODELING OF TIME-LOCALIZED FREQUENCIES

We introduce a wavelet-based tokenizer that allows the model to learn complex representations directly in the space of time-localized frequencies. Our method first scales and decomposes the input time series, then thresholds and quantizes the wavelet coefficients, and finally it pre-trains an autoregressive model to forecast wavelet coefficients for the horizon window.

#### 3.1 A BRIEF TOUR OF WAVELETS

Here we provide a very brief introduction to the main concepts and terminology regarding wavelets. See Appendix A and references therein for more details. The Wavelet transform (WT) was intro-

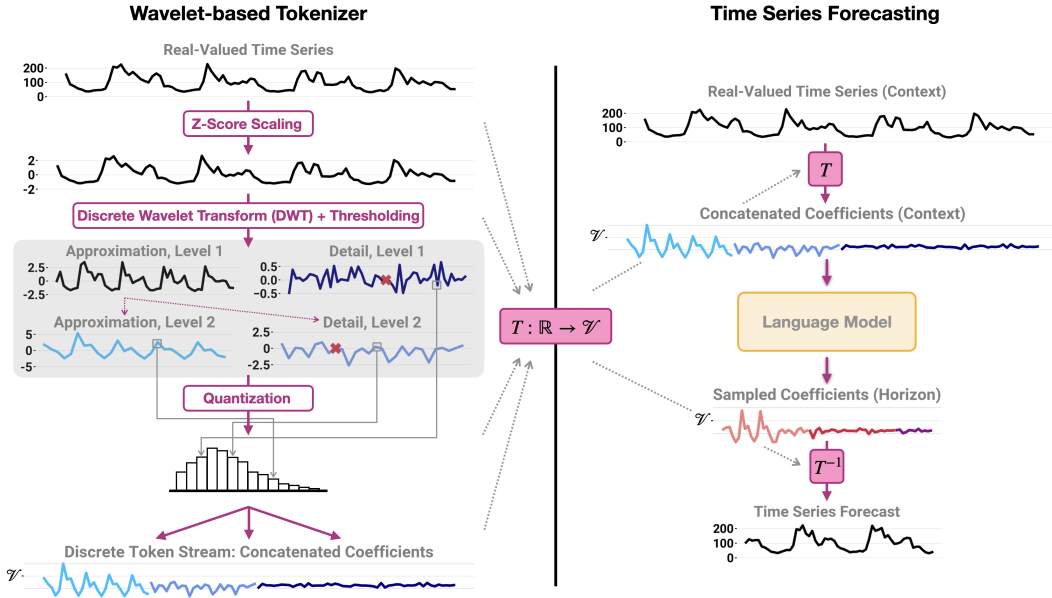


Figure 2: **High-level depiction of our method.** (Left) WaveToken first re-scales the input time series by computing  $\tilde{x}_t = (x_t - \mu_{1:C})/\sigma_{1:C}$ , then it applies the DWT and possibly thresholds the resulting detail coefficients to zero (red crosses). The wavelet coefficients are finally quantized to bins of optimal size given their empirical distribution, and then concatenated together (excluding the first  $J - 1$  approximations). (Right) After pretraining on a large corpus of time series, at inference time the model samples autoregressively from the categorical output distribution and yields coefficients at all decomposition levels, which are pushed through the inverse tokenizer to obtain a forecast.

duced to address some limitations in existing mathematical tools — namely the Fourier transform, which implicitly assumes a signal is stationary — by employing a quickly decaying zero-mean oscillatory function, known as the mother wavelet, which inherently adapts its time-frequency resolution to the signal’s characteristics. This dual localization property, achieved through the modulation of the wavelet’s scale parameter, enables the WT to efficiently analyze non-stationary signals achieving localization in both time and frequency domain (Daubechies, 1992; Mallat, 2009).

We can divide wavelet families into two sets of basis functions: the father wavelet, which captures low frequencies (the *approximation*), and the mother wavelet, which focuses on high frequencies (the *detail*). Both sets can be modulated via scaling and translation to achieve a multi-resolution decomposition of an arbitrary signal  $f(x)$  into the  $J$ -th lowest approximation component combined with the  $J - 1$  successive details. In what follows, we obtain approximation  $\{a_k\}_J$  and detail coefficients  $\{d_k\}_j, \forall k, j$  via the maximally decimated Discrete Wavelet Transform (DWT), which decomposes a signal and preserves its length  $N$  by applying a cascade of high-pass and low-pass conjugate mirror filters via successive convolutions and down-sampling operations in  $\mathcal{O}(N)$  time.

### 3.2 TOKENIZATION VIA WAVELET DECOMPOSITION

We ask the following question: given a real-valued univariate time series  $\mathbf{x}_{1:C} = [x_1, \dots, x_C]$ , where  $C$  is the context length, can we find an optimal map  $T : \mathbb{R} \rightarrow \mathcal{V}$  that encodes the input with a compact but expressive *discrete* vocabulary  $\mathcal{V}$ ? To this end, we develop WaveToken, a tokenization pipeline divided in scaling, wavelet decomposition, thresholding and quantization. See Section 4.4 for an extensive analysis of the chosen hyper-parameters.

**Scaling.** Re-normalizing time series is standard practice in modern forecasting, as it brings all inputs to a common scale and avoids numerical and optimization issues, especially for globally-learned deep learning models (Benidis et al., 2022). Popular normalization techniques are based on affine transformations  $\tilde{x}_t = (x_t - m)/s$ , with  $m$  and  $s$  appropriately chosen. We set  $m =$

216  $\mu_{1:C} = \frac{1}{C} \sum_{t=1}^C x_t$  and  $s = \sigma_{1:C} = \sqrt{\frac{1}{C-1} \sum_{t=1}^C (x_t - \mu_{1:C})^2}$ , also known as z-score scaling.  
 217 This choice is especially important in our case because the specific wavelet transform we adopt is  
 218 not translation-invariant, hence a shift in the input signal can lead to different coefficients. Other  
 219 popular normalization techniques — e.g., dividing by the mean of the absolute values in the context  
 220 — could therefore yield unexpected results for similar inputs. By applying this transformation, we  
 221 make sure the model receives consistent time-frequency representations.  
 222

223 **Decomposition.** We then apply the *maximally decimated* DWT (Daubechies, 1992) to decompose  
 224 the scaled time series  $\tilde{x}_{1:C}$  into its constituent time-localized frequencies up to the  $J$ -th level, which  
 225 yields approximation coefficients  $\{a_k\}_J$  and a series of detail coefficients  $\{d_k\}_{j=1}^J, \forall k$ . In addition  
 226 to being faster than the FFT as mentioned in Section A.2, this wavelet transform leads to compact  
 227 representations since it preserves the input size — i.e., a signal of size  $N$  results in  $N$  coefficients<sup>1</sup>  
 228 — and tends to concentrate the majority of the signal energy onto only a few significant wavelet  
 229 coefficients. This is especially true for time series with sharp spikes or localized features, and  
 230 is a useful property for compression and denoising. As each coefficient group is the outcome of  
 231 convoluting a filter with the signal, the autoregressive structure is also preserved *within* each group.  
 232

233 **Thresholding.** The inherently sparse representations that the DWT induces imply that we can  
 234 encode complex features with only a few significant wavelet coefficients, while the rest are close to  
 235 zero and thus can potentially be discarded without significantly addressing reconstruction quality.  
 236 Several thresholding techniques, many tailored to specific applications, have been developed over the  
 237 years and are effectively used in practice (e.g., in image compression: Chang et al. (2000); Vetterli  
 238 & Kovacevic (1995); Christopoulos et al. (2000)). As the main downstream task in this work is  
 239 to pre-train a language model on a large corpus of diverse time series datasets, any thresholding  
 240 technique must be adaptive to the underlying noise and complexity level of the input, so as to retain  
 241 most of the signal energy without discarding essential information. In what follows, we always keep  
 242 the approximation coefficients unaltered since they model the low-resolution coarse structure of the  
 243 time series, and explore the following techniques for thresholding detail coefficients:  
 244

244 *No-thresholding:*  $\bar{d}_{k,j} = d_{k,j}$ . If the chosen wavelet family preserves signal energy (in the sense of  
 Parseval’s theorem), not thresholding the coefficients avoids any information loss at this stage.

246 *CDF-thresholding:*  $\bar{d}_{k,j} = d_{k,j} \mathbf{1}\{|d_{k,j}| > F_{|d_j|}^{-1}(b^{J-j+1})\}$ . A coefficient is set to 0 if it is in the  
 247 lower tail of the empirical distribution of the details’ magnitude at the corresponding  $j$ -th level,  
 248 where the cutoff grows exponentially from coarser to finer coefficients to reflect granularity and  
 249 downsampling of the DWT.

250 *VisuShrink (Donoho, 1995):*  $\bar{d}_{k,j} = \text{sign}(d_{k,j})(|d_{k,j}| - \lambda)$ , with  $\lambda = \sigma\sqrt{2\log N}$  and  $\sigma$  estimated  
 251 from the finest detail coefficients  $d_{k,j=1}$ . The DWT of noisy data can be seen as a maximum-  
 252 likelihood estimate of the wavelet coefficients, and it can be shown that this threshold reduces the  
 253 expected reconstruction error (i.e., estimator’s risk) close to the possible minimum, under certain  
 254 assumptions. We explore both the soft- and hard-thresholding variants of this method.

255 *FDRC (Abramovich & Benjamini, 1996):* see Appendix B for details on the algorithm. By leverag-  
 256 ing the connection between thresholding and multiple hypotheses testing, this procedure improves  
 257 on *VisuShrink* by adaptively choosing  $\lambda$  to control the expected proportion of incorrectly included  
 258 coefficients (similar to false discovery rate) among those chosen for the wavelet reconstruction.

259 See Section 4.4 and Appendix B for results and justifications on the chosen thresholding technique.  
 260

261 **Quantization.** At this point, the resulting coefficients  $\{a_k\}_J$  and  $\{\bar{d}_k\}_{j=1}^J$  are still real-valued and  
 262 need to be converted into discrete tokens to be directly processed by language models. We construct  
 263 the vocabulary  $\mathcal{V}$  by binning the raw coefficients according to their joint empirical distribution on  
 264 the training set, and choose the optimal bin size according to the Freedman-Diaconis rule (FD) to  
 265 minimize the reconstruction error (Freedman & Diaconis, 1981). In symbols, given the optimal  $B$   
 266 bin centers  $c_1 < \dots < c_B$  and  $B-1$  edges  $c_i < e_i < c_{i+1}$  for  $i = 1, \dots, B-1$ , we map each  
 267 wavelet coefficient  $w \in \{\{a_k\}_J, \{\bar{d}_k\}_j\}$  to  $\mathcal{V}$  as follows:  $q(w) = i \cdot \mathbf{1}\{e_{i-1} \leq w < e_i\}$ . We  
 268

269 <sup>1</sup>To be precise, longer filters and specific boundary conditions to handle the signal edges might yield a  
 slightly higher number of coefficients (Torrence & Compo, 1998).

further enrich  $\mathcal{V}$  to be immediately compatible with language models by adding two special tokens: a PAD token that signals missing values in the wavelet coefficients — resulting from missing values in the time series or from padding of short instances — and an EOS token that signals the end of the sequence. In our context, a single shared vocabulary jointly encodes time-localized low and high frequencies, thereby leading to a compressed but expressive codebook.

### 3.3 MODEL TRAINING, OBJECTIVE FUNCTION AND FORECASTING

Given a time series context  $\mathbf{x}_{1:C}$ , we apply the steps detailed in Section 3.2 and then concatenate the resulting discrete tokens for approximation and detail coefficients into a vector  $\mathbf{z}_{1:C} = [\mathbf{a}_J, \mathbf{d}_J, \dots, \mathbf{d}_1]$ , so that the model can learn and forecast coarse-to-fine structures in a multi-scale fashion. To minimize ad-hoc modifications to the language model, we opt for an encoder-decoder architecture based on the T5 family (Raffel et al., 2020), which has recently been shown to achieve excellent zero-shot performance on a comprehensive benchmark (Ansari et al., 2024). Other proposed LLM-based forecasters either reformulate the problem as a question-answering task or use patches of the input as tokens, and would therefore not be immediately compatible with our wavelet-based tokenizer (see section 2 for an exhaustive review). For brevity, in what follows we refer to WaveToken as being both the tokenizer and the model paired together.

We train the model via next-token prediction by minimizing the cross-entropy between the predicted distribution and the categorical output distribution over the corresponding label tokens obtained from the horizon window  $\mathbf{z}_{C:C+H}$ . In symbols, the loss function for a time series (including EOS) is

$$l_\theta = - \sum_{h=1}^{H+1} \sum_{i=1}^{|\mathcal{V}|} \mathbf{1}\{z_{C+h+1} = i\} \log p_\theta(z_{C+h+1} = i \mid \mathbf{z}_{1:C+h})$$

While the cross-entropy loss does not induce a metric onto the underlying vocabulary, it offers greater flexibility to learn output distributions of arbitrary shapes. This property lends itself well to forecasting applications, where it is often important to capture the correct shape or pattern of the time series without imposing structural limitations such as those inherent in traditional loss functions like MSE and MAE (Le Guen & Thome, 2019).

Learning an autoregressive model on concatenated groups of wavelet coefficients might seem counter-intuitive: the temporal structure is only preserved within each coefficient group and is broken as the input transitions from, e.g., approximations to details. In practice, this turns out to be surprisingly helpful as it offers the model a natural way to break down complex sub-structures in inputs and outputs by dividing them into a hierarchy of time-localized frequency bands. As we will see in Section 4.3, the model easily learns to exploit these partitions and is able to attend to the right coefficients to improve the overall forecasting accuracy.

At inference time, the model produces sample paths over the vocabulary via autoregressive sampling from the predicted distribution  $p_\theta(z_{C+h+1} \mid \mathbf{z}_{1:C+h})$ ,  $h = 1, \dots, H$ . To obtain a time series forecast, we first de-quantize the tokens by mapping them to the corresponding bin center:  $q^{-1}(i) = c_i$ . We then apply the inverse discrete wavelet transform (IDWT) and un-scale the reconstructed series by multiplying it by  $\sigma_{1:C}$  and adding  $\mu_{1:C}$ , as depicted in Figure 2.

## 4 EXPERIMENTS

### 4.1 SETUP OF EMPIRICAL EVALUATION

**Models and baselines.** We pre-train WaveToken with T5 models of four sizes<sup>2</sup> — Mini (19.2M), Small (44.5M), Base (199M) and Large (705.8M) — for 200K steps on 8 A100 GPUs, and we compare their performance against *i*) popular task-specific models trained for each dataset separately, namely DeepAR (Salinas et al., 2020), PatchTST (Nie et al., 2022) and TFT (Lim et al., 2021); and *ii*) recently proposed foundation models for time series forecasting — namely, TimesFM (Das et al., 2023), Chronos Mini-Large (Ansari et al., 2024), Moirai Base & Large (Woo et al., 2024), and Lag-llama (Rasul et al., 2023) — which do not perform task-specific training, but are trained only

<sup>2</sup>Parameter counts were obtained with the optimal vocabulary size as detailed in Section 4.4.

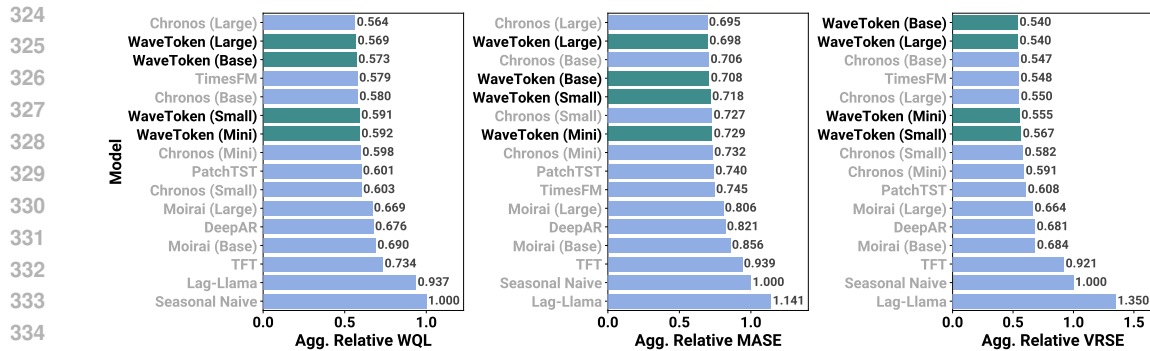


Figure 3: WaveToken performs on par or better than other baselines on in-domain datasets. Forecasting accuracy on Benchmark I in terms of WQL, MASE and VRSE.

once on a large corpus and then deployed across all evaluation datasets. Appendix G details all the hyper-parameters for the mentioned baselines.

**Datasets and training strategy.** We train and evaluate WaveToken on the publicly available datasets comprehensively collected by Ansari et al. (2024). These span a variety of domains and exhibit diverse properties in terms of size, frequencies and prediction lengths, and can be divided in *i) pre-training only*: datasets exclusively used for training (13 datasets); *ii) in-domain*: datasets employed for training, whose validation set is also used for evaluation (Benchmark I, 15 datasets); and *iii) zero-shot*: datasets used solely for evaluation (Benchmark II, 27 datasets). See Appendix G for detailed information about all datasets. The context length of the sequences in each training batch is set to 512 and the prediction length is set to 64. In addition, we adopt the data augmentations techniques introduced by Ansari et al. (2024): each of the sequences is generated with probability 0.9 from a TSMixup set, which takes convex combinations of different time series, and with probability 0.1 from a synthetic dataset generated from Gaussian Processes based on randomly combined kernels. Both of these have been shown to be effective in domains such as time series forecasting, where data is inherently scarce relative to standard language modeling applications.

**Evaluation tasks and metrics.** For both in-domain (I) and zero-shot (II) benchmark datasets, we use the last  $H$  observations of each time series as a held-out test set. We compute the weighted quantile loss (WQL) to assess the quality of probabilistic forecasts on 9 uniformly-spaced quantile levels  $\{0.1, 0.2, \dots, 0.9\}$  and the mean absolute scaled error (MASE; Hyndman & Koehler (2006)) to evaluate the quality of point forecasts. In addition, we compute the Visual Relative Squared Error (VRSE; Posam et al. (2024)), which measures the relative squared difference of the amplitudes at all frequencies between the ground truth and the (median) forecast. This metric serves a complementary role to avoid common pitfalls of standard scores, which can fail to properly assess important edge cases that would otherwise be visually obvious, as shown in Figure 9. In order to aggregate these metrics and provide fair comparisons, we compute each model’s score divided by the score of a baseline model (here, Seasonal Naive). These relative scores are then aggregated across all datasets using the geometric mean. See Appendix C for more details. All results for Chronos and WaveToken are averaged across three different seeds.

## 4.2 IN-DOMAIN & ZERO-SHOT BENCHMARKS

Figure 3 summarizes the forecasting performance of all models on the in-domain datasets of Benchmark I. WaveToken outperforms all other baselines with the exception of Chronos-Large on WQL and MASE, and is superior with respect to VRSE. Considering each model size for each metric, WaveToken achieves lower (i.e., better) scores than Chronos 75% of the times and largely improves on other recent LLM-based forecasters. Similarly, our method is considerably better even than task-specific models trained separately on each dataset. Note again that WaveToken uses a vocabulary size of 1024, while Chronos, for example, uses four times as much tokens with  $|\mathcal{V}| = 4096$ . This empirical finding confirms the well-known theoretical properties of wavelets, which can provide compact but very expressive representations able to condense complex structures into a compressed

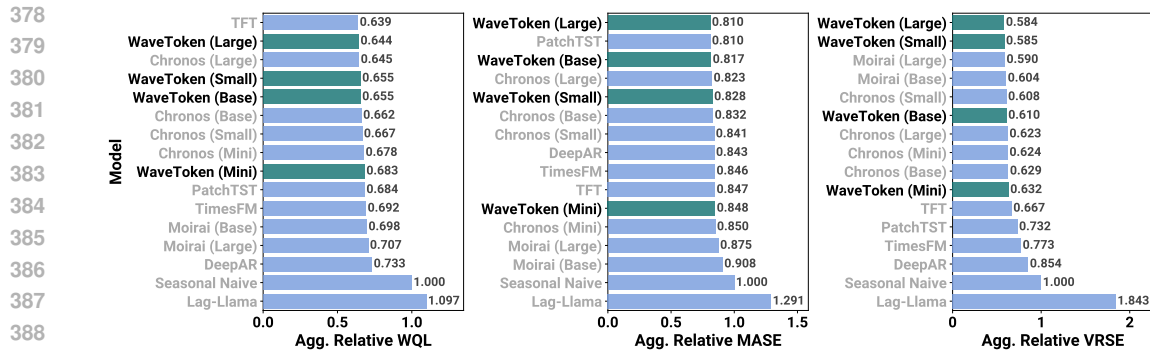


Figure 4: WaveToken performs on par or better even relative to task-specific models on zero-shot datasets. Forecasting accuracy on Benchmark II in terms of WQL, MASE and VRSE.

codebook. Finally, on the datasets of Benchmark I, WaveToken achieves the best average rank across all metrics, as shown in Figure 10.

Benchmark II focuses on the forecasting performance on datasets that were never included in the training corpus (for brevity, zero-shot). As shown in Figure 4, WaveToken exhibits superior generalization capabilities which lead it to *i)* outperform all other foundation models for time series across all metrics, with a 83% success rate against Chronos models of the same size; and *ii)* be competitive on WQL and MASE, and much better on VRSE, relative to task-specific models specifically trained on each zero-shot dataset. Again, WaveToken achieves the best average rank across all metrics on the dataset of Benchmark II, as shown in Figure 11.

Figure 12 in Appendix E shows results on a long-horizon benchmark constructed by increasing the forecast length  $H$  of each dataset in Benchmark II (Zero-Shot) by a factor of 2 and 3. WaveToken outperforms other foundation models across almost all combinations of metrics and long horizons, the only exception being  $H \times 3$  with respect to WQL, where TimesFM performs slightly better. Appendix D shows the raw WQL, MASE and VRSE values for each dataset in Benchmark I and II.

### 4.3 QUALITATIVE ANALYSIS

So far we have seen how wavelets allow a transformer-based architecture trained on a large corpus to achieve excellent forecasting performance especially on previously unseen datasets, which hints at their superior generalization capabilities. It is then worth analyzing more deeply some edge cases of practical relevance to showcase how wavelets can efficiently capture a wide variety of complex patterns, frequencies and local structures within a compressed representation. Figure 1 shows examples of synthetically-generated time series which exhibit strong trends, sharp spikes and several frequencies evolving over time. We evaluate WaveToken against popular recent foundation models for time series forecasting. Both Chronos, TimesFM and Moirai clearly underestimate trends, struggle at isolating sudden spikes and are not able to capture non-stationary behaviours. On the other hand, our model is able to leverage the different concatenated coefficient groups which represent the time-localized frequency bands, thereby providing accurate forecasts with very low uncertainty.

This phenomenon can be further explained by looking at patterns in the cross-attention layers of Chronos and our model, as they use the same T5 encoder-decoder architectures. Figure 5 shows heat-maps of the cross-attention weights in the eighth decoder layer of Chronos-Base (left) and WaveToken-Base (right), when forecasting the sparse spikes in the second row of Figure 1. Two main things are worth noticing: first of all the attention map for our model is clearly divided in four quadrants, of which the upper-left and lower-right ones exhibit generally larger attention values. These clearly show that, to forecast approximation coefficients in the horizon (time-steps 0-34 on the  $x$ -axis), the model is learning to attend more to approximation coefficients in the context (time-steps 0-258 on the  $y$ -axis), and to forecast detail coefficients in the future (time-steps 35-68 on the  $x$ -axis), the model attends more to detail coefficients in the context (time-steps 259-516 on the  $y$ -axis). Second, we notice an interesting pattern: the detail coefficients for the horizon present two

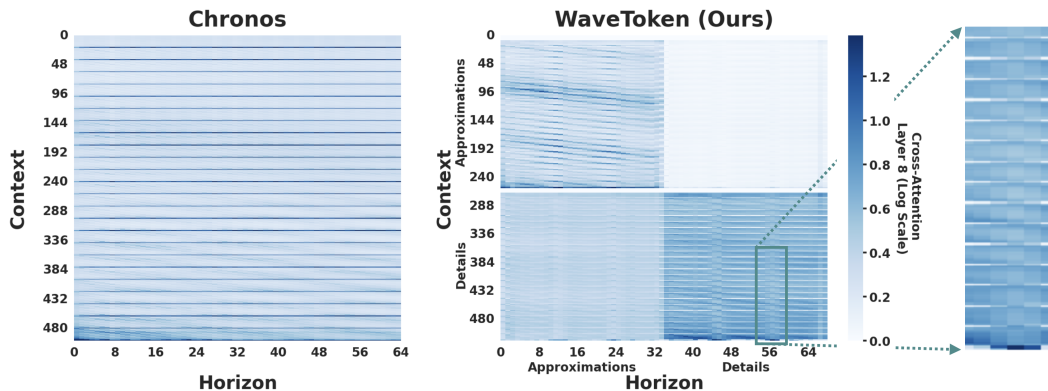


Figure 5: **Wavelet-based tokenization induces structured patterns in the cross-attention maps.** Cross-attention weights for the eighth decoder layer when forecasting the spiky data of Figure 1 (second row). Chronos-Base (left) repeats the same patterns for all steps, while WaveToken-Base (right) shows high values at the detail coefficients corresponding to the spikes.

clear columns of larger attention weights (time-steps 45 and 56 on the  $x$ -axis) that map to the detail coefficients representing the spikes in the context. In addition, other detail coefficients attend to everywhere else in the bottom-right quadrant (corresponding to the flat regions in time domain for the spiky data of Figure 1) except to those same positions corresponding to spikes (see the white horizontal lines interrupted by the vertical column in the magnified portion). Similar patterns are present for the approximation coefficients, albeit less defined. None of this structures is present in the attention weights of Chronos-Base shown in the left panel, which repeats the same patterns for all steps and indeed fails to forecast the correct position and intensity of the spikes in time domain.

Appendix F shows the remaining attention maps for layers missing in Figure 5, which all show similar patterns with varying intensities.

#### 4.4 ABLATION STUDY

Figure 6 shows the effect of different vocabulary sizes, wavelet families and decomposition levels on the forecasting accuracy of WaveToken-Small trained for 200K steps on one A100 GPU. Regarding *vocabulary size*, which determines the precision with which tokens encode wavelet coefficients, we observe a gradual but consistent improvement until  $|\mathcal{V}| = 1024$ , which we select as the optimal value. For higher vocabulary sizes, WQL and MASE remain flat or worsen on both in-domain and zero-shot benchmarks. This phenomenon can be ascribed to the intrinsic compression properties of wavelets (Mallat, 2009): by concentrating most of the signal energy onto a few coefficients, we can effectively capture more information with a smaller codebook, while a larger one would only reserve more tokens to spurious coefficients. Note that our vocabulary is much smaller than comparable models: Chronos for example, that leverages the same architectures, uses  $|\mathcal{V}| = 4096$ . As to the many *wavelet families* available, the central panel of Figure 6 shows that the Biorthogonal-2.2 basis achieves optimal performance. This family uses two separate filters with two vanishing moments for analysis and synthesis, a dual structure that allows for symmetric or near-symmetric wavelet functions that help preventing distortions near the signal edges. This is known to be advantageous in many applications, including image compression<sup>3</sup>. Families with higher vanishing moments capable of capturing higher order polynomial did not prove effective. As to the *decomposition level*, we observe that first-level coefficients are sufficient to achieve good forecasting accuracy. Albeit deeper levels provide more granular time-localized frequencies, the higher number of groups in the concatenated coefficients make it harder for the attention mechanism to identify the relevant ones at each prediction step. Regarding *thresholding*, we analyze the performance of all four techniques described in Section 3. Empirically, we observe a discrepancy in the results obtained when training

<sup>3</sup>Biorthogonal wavelets with the maximally decimated DWT are in fact used in popular compression standards, such as JPEG-2000 (Christopoulos et al., 2000; Usevitch, 2001).

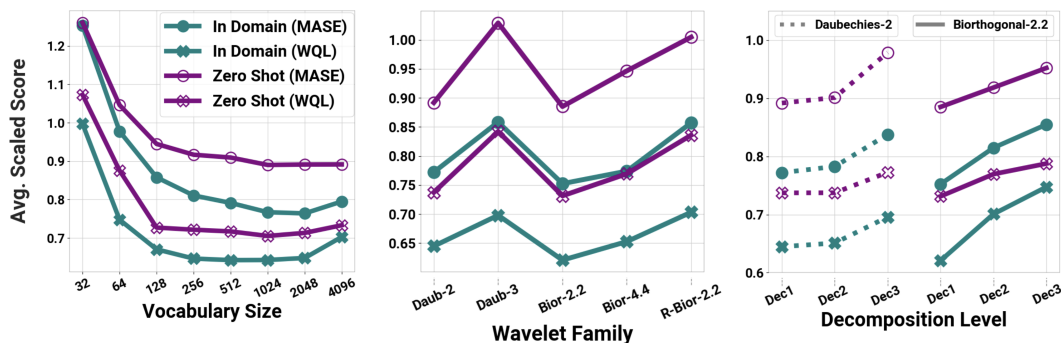


Figure 6: **Effect of different vocabulary sizes, wavelet families and decomposition levels on downstream forecasting accuracy of WaveToken-Small.** The optimal hyper-parameters were a single-level wavelet decomposition with a Biorthogonal-2.2 family and a vocabulary size of 1024. See Section 4 for more details.

for the same number of steps on 1 or 8 GPUs, where the latter is the final configuration used to train the optimal models. As Figure 8 shows, in the single-GPU setting, chosen to streamline computations during hyper-parameter optimization, *VisuShrink* (Donoho, 1995) appears to be the best, a result which is then reverted in favor of *No-thresholding* in the 8-GPU setting, which increases the total number of samples processed at each step, thereby allowing the model to learn the richer frequencies preserved in the input. *VisuShrink*, on the other hand, leads to smoother signals by crudely cutting off coefficients, which eventually harms generalization. These empirical observations led us to not threshold coefficients, although we note that thresholding is still implicitly happening during the *quantization* step, which collapses small coefficients to the bin centered at 0. This value is then used at inference time to forecast tokens mapped to this bin. Optimal bins for the discretization procedure — detailed in Section 3 — were selected between the lower and upper bounds  $[-30, 30]$ , chosen empirically by scanning the training corpus.

## 5 CONCLUSION

In this work, we develop WaveToken, a tokenization pipeline tailored to a specific goal: constructing a general-purpose forecasting model capable of capturing a wide variety of complex patterns while consuming as little information as possible, thereby leading to excellent generalization performance on unseen datasets. We leverage a recently-proposed framework to pre-train an encoder-decoder architecture in the context of time series (Ansari et al., 2024) and re-purpose it to learn an autoregressive model in the space of time-localized frequencies. The resulting wavelet-based vocabulary is both compact — using 1024 tokens, i.e. one quarter of Chronos — and very expressive, and leads to

*i)* excellent **forecasting accuracy** with respect to all other baselines in terms of three complementary metrics: weighted quantile loss for probabilistic forecasts, mean absolute scaled error for point forecasts, and visual relative squared error to measure discrepancies in the frequency content relative to the ground truth.

*ii)* superior **generalization** capabilities, with WaveToken being the best model across all datasets and metrics in terms of average rank. In addition, our method can easily capture complex temporal patterns in several edge cases relevant for practical applications, as shown in Figure 1.

As potential future directions, we foresee that exploring techniques to automatically handle context lengths larger than 512 in the tokenizer would allow models to capture longer-range dependencies if needed. The DWT is in fact a natural tool to leverage in these settings, as it can encode long contexts without increasing the input length through convolutions and down-sampling. Furthermore, WaveToken exploits an autoregressive model on wavelet coefficients. As such, it suffers from slower decoding and inference times relative to recently proposed alternatives, such as patch-based models. Applying WaveToken to patch-based architectures represents an interesting area for future research.

540  
541  
542  
543  
544  
545  
546  
547  
548  
549  
550  
551  
552  
553  
554  
555  
556  
557  
558  
559  
560  
561  
562  
563  
564  
565  
566  
567  
568  
569  
570  
571  
572  
573  
574  
575  
576  
577  
578  
579  
580  
581  
582  
583  
584  
585  
586  
587  
588  
589  
590  
591  
592  
593

## REFERENCES

- Felix Abramovich and Yoav Benjamini. Adaptive thresholding of wavelet coefficients. *Computational Statistics & Data Analysis*, 22(4):351–361, 1996. 5, 16
- Alexander Alexandrov, Konstantinos Benidis, Michael Bohlke-Schneider, Valentin Flunkert, Jan Gasthaus, Tim Januschowski, Danielle C Maddix, Syama Rangapuram, David Salinas, Jasper Schulz, et al. Gluonts: Probabilistic and neural time series modeling in python. *Journal of Machine Learning Research*, 21(116):1–6, 2020. 21
- Zaid Alyafeai, Maged S Al-shaibani, Mustafa Ghaleb, and Irfan Ahmad. Evaluating various tokenizers for arabic text classification. *Neural Processing Letters*, 55(3):2911–2933, 2023. 3
- Abdul Fatir Ansari, Lorenzo Stella, Caner Turkmen, Xiyuan Zhang, Pedro Mercado, Huibin Shen, Oleksandr Shchur, Syama Sundar Rangapuram, Sebastian Pineda Arango, Shubham Kapoor, et al. Chronos: Learning the language of time series. *arXiv preprint arXiv:2403.07815*, 2024. 1, 2, 3, 6, 7, 10, 21, 25
- Konstantinos Benidis, Syama Sundar Rangapuram, Valentin Flunkert, Yuyang Wang, Danielle Maddix, Caner Turkmen, Jan Gasthaus, Michael Bohlke-Schneider, David Salinas, Lorenzo Stella, et al. Deep learning for time series forecasting: Tutorial and literature survey. *ACM Computing Surveys*, 55(6):1–36, 2022. 1, 4
- Tom B Brown. Language models are few-shot learners. *arXiv preprint arXiv:2005.14165*, 2020. 3
- S Grace Chang, Bin Yu, and Martin Vetterli. Adaptive wavelet thresholding for image denoising and compression. *IEEE transactions on image processing*, 9(9):1532–1546, 2000. 5
- Seokmin Choi, Sajad Mousavi, Phillip Si, Haben G Yhdego, Fatemeh Khadem, and Fatemeh Afghah. Ecgbert: Understanding hidden language of ecgs with self-supervised representation learning. *arXiv preprint arXiv:2306.06340*, 2023. 3
- Charilaos Christopoulos, Athanassios Skodras, and Touradj Ebrahimi. The jpeg2000 still image coding system: an overview. *IEEE transactions on consumer electronics*, 46(4):1103–1127, 2000. 5, 9
- Gautier Dagan, Gabriel Synnaeve, and Baptiste Roziere. Getting the most out of your tokenizer for pre-training and domain adaptation. In *Proceedings of the 41st International Conference on Machine Learning*, volume 235, pp. 9784–9805. PMLR, 2024. 1
- Abhimanyu Das, Weihao Kong, Rajat Sen, and Yichen Zhou. A decoder-only foundation model for time-series forecasting. *arXiv preprint arXiv:2310.10688*, 2023. 1, 2, 3, 6, 21
- Ingrid Daubechies. *Ten lectures on wavelets*. SIAM, 1992. 4, 5, 15
- David L Donoho. De-noising by soft-thresholding. *IEEE transactions on information theory*, 41(3): 613–627, 1995. 5, 10
- David Freedman and Persi Diaconis. On the histogram as a density estimator: L 2 theory. *Zeitschrift für Wahrscheinlichkeitstheorie und verwandte Gebiete*, 57(4):453–476, 1981. 5
- Philip Gage. A new algorithm for data compression. *The C Users Journal*, 12(2):23–38, 1994. 3
- Federico Garza, Max Mergenthaler Canseco, Cristian Challú, and Kin G Olivares. Statsforecast: Lighting fast forecasting with statistical and econometric models. *PyCon: Salt Lake City, UT, USA*, 2022. 21
- Siavash Golkar, Mariel Pettee, Michael Eickenberg, Alberto Bietti, Miles Cranmer, Geraud Krawezik, Francois Lanusse, Michael McCabe, Ruben Ohana, Liam Parker, et al. xval: A continuous number encoding for large language models. *arXiv preprint arXiv:2310.02989*, 2023. 3
- Tobias Golling, Lukas Heinrich, Michael Kagan, Samuel Klein, Matthew Leigh, Margarita Osadchy, and John Andrew Raine. Masked particle modeling on sets: Towards self-supervised high energy physics foundation models. *Machine Learning: Science and Technology*, 5(3):035074, 2024. 1

---

594 Mononito Goswami, Konrad Szafer, Arjun Choudhry, Yifu Cai, Shuo Li, and Artur Dubrawski.  
595 Moment: A family of open time-series foundation models. *arXiv preprint arXiv:2402.03885*,  
596 2024. 3

597 Nate Gruver, Marc Finzi, Shikai Qiu, and Andrew G Wilson. Large language models are zero-shot  
598 time series forecasters. *Advances in Neural Information Processing Systems*, 36, 2024. 3

600 Florentin Guth, Simon Coste, Valentin De Bortoli, and Stephane Mallat. Wavelet score-based gen-  
601 erative modeling. *Advances in neural information processing systems*, 35:478–491, 2022. 3

602 Alfred Haar. Zur theorie der orthogonalen funktionensysteme. *Mathematische Annalen*, 71(1):  
603 38–53, 1911. 15

605 Rob J Hyndman and Anne B Koehler. Another look at measures of forecast accuracy. *International*  
606 *journal of forecasting*, 22(4):679–688, 2006. 7, 17

607 Ming Jin, Shiyu Wang, Lintao Ma, Zhixuan Chu, James Y Zhang, Xiaoming Shi, Pin-Yu Chen, Yux-  
608 uan Liang, Yuan-Fang Li, Shirui Pan, et al. Time-llm: Time series forecasting by reprogramming  
609 large language models. *arXiv preprint arXiv:2310.01728*, 2023. 3

611 Roger Koenker and Kevin F Hallock. Quantile regression. *Journal of economic perspectives*, 15(4):  
612 143–156, 2001. 17

613 Pedro Lara-Benítez, Manuel Carranza-García, and José C Riquelme. An experimental review on  
614 deep learning architectures for time series forecasting. *International journal of neural systems*,  
615 31(03):2130001, 2021. 1

616 Vincent Le Guen and Nicolas Thome. Shape and time distortion loss for training deep time series  
617 forecasting models. *Advances in neural information processing systems*, 32, 2019. 6

618 Bryan Lim, Sercan Ö Arık, Nicolas Loeff, and Tomas Pfister. Temporal fusion transformers for  
619 interpretable multi-horizon time series forecasting. *International Journal of Forecasting*, 37(4):  
620 1748–1764, 2021. 6

621 Stéphane Mallat. *A Wavelet Tour of Signal Processing: The Sparse Way*. Academic Press, 3rd  
622 edition, 2009. 2, 4, 9, 15, 16

623 Stéphane G Mallat. Multiresolution approximations and wavelet orthonormal bases of  $L^2(\mathbb{R})$ .  
624 *Transactions of the American mathematical society*, 315(1):69–87, 1989. 16

625 Wael Mattar, Idan Levy, Nir Sharon, and Shai Dekel. Wavelets are all you need for autoregressive  
626 image generation. *arXiv preprint arXiv:2406.19997*, 2024. 3

627 Yves Meyer. *Wavelets and operators: volume 1*. Cambridge university press, 1992. 16

628 Suvir Mirchandani, Fei Xia, Pete Florence, Brian Ichter, Danny Driess, Montserrat Gonzalez Are-  
629 nas, Kanishka Rao, Dorsa Sadigh, and Andy Zeng. Large language models as general pattern  
630 machines. *arXiv preprint arXiv:2307.04721*, 2023. 1

631 Yuqi Nie, Nam H Nguyen, Phanwadee Sinthong, and Jayant Kalagnanam. A time series is worth 64  
632 words: Long-term forecasting with transformers. *arXiv preprint arXiv:2211.14730*, 2022. 6

633 Alan V. Oppenheim and Ronald W. Schaffer. *Discrete-Time Signal Processing*. Pearson, 2010. 15

634 Spiros Papadimitriou, Anthony Brockwell, and Christos Faloutsos. Adaptive, hands-off stream min-  
635 ing. In *Proceedings 2003 VLDB Conference*, pp. 560–571. Elsevier, 2003. 3

636 Lalithsai Posam, Shubhranshu Shekhar, Meng-Chieh Lee, and Christos Faloutsos. Diffind: Discov-  
637 ering differential equations from time series. In *Pacific-Asia Conference on Knowledge Discovery*  
638 *and Data Mining*, pp. 175–187. Springer, 2024. 7, 17

639 Hendrik Purwins, Bo Li, Tuomas Virtanen, Jan Schlüter, Shuo-Yiin Chang, and Tara Sainath. Deep  
640 learning for audio signal processing. *IEEE Journal of Selected Topics in Signal Processing*, 13  
641 (2):206–219, 2019. 3

---

648 Colin Raffel, Noam Shazeer, Adam Roberts, Katherine Lee, Sharan Narang, Michael Matena, Yanqi  
649 Zhou, Wei Li, and Peter J Liu. Exploring the limits of transfer learning with a unified text-to-text  
650 transformer. *Journal of machine learning research*, 21(140):1–67, 2020. 2, 6  
651

652 Kashif Rasul, Arjun Ashok, Andrew Robert Williams, Arian Khorasani, George Adamopoulos,  
653 Rishika Bhagwatkar, Marin Biloš, Hena Ghonia, Nadhir Vincent Hassen, Anderson Schnei-  
654 der, et al. Lag-llama: Towards foundation models for time series forecasting. *arXiv preprint*  
655 *arXiv:2310.08278*, 2023. 3, 6, 21

656 David Salinas, Valentin Flunkert, Jan Gasthaus, and Tim Januschowski. Deepar: Probabilistic fore-  
657 casting with autoregressive recurrent networks. *International journal of forecasting*, 36(3):1181–  
658 1191, 2020. 6  
659

660 Lena Sasal, Tanujit Chakraborty, and Abdenour Hadid. W-transformers: a wavelet-based trans-  
661 former framework for univariate time series forecasting. In *2022 21st IEEE international confer-*  
662 *ence on machine learning and applications (ICMLA)*, pp. 671–676. IEEE, 2022. 3

663 Aaditya K Singh and DJ Strouse. Tokenization counts: the impact of tokenization on arithmetic in  
664 frontier llms. *arXiv preprint arXiv:2402.14903*, 2024. 2  
665

666 Gilbert Strang and Truong Nguyen. *Wavelets and filter banks*. SIAM, 1996. 15  
667

668 Shashank Subramanian, Peter Harrington, Kurt Keutzer, Wahid Bhimji, Dmitriy Morozov,  
669 Michael W Mahoney, and Amir Gholami. Towards foundation models for scientific machine  
670 learning: Characterizing scaling and transfer behavior. *Advances in Neural Information Process-*  
671 *ing Systems*, 36, 2024. 1

672 Sabera Talukder, Yisong Yue, and Georgia Gkioxari. Totem: Tokenized time series embeddings for  
673 general time series analysis. *arXiv preprint arXiv:2402.16412*, 2024. 3  
674

675 Keyu Tian, Yi Jiang, Zehuan Yuan, Bingyue Peng, and Liwei Wang. Visual autoregressive modeling:  
676 Scalable image generation via next-scale prediction. *arXiv preprint arXiv:2404.02905*, 2024. 3

677 Arseny Tolmachev, Daisuke Kawahara, and Sadao Kurohashi. Juman++: A morphological analysis  
678 toolkit for scriptio continua. In *Proceedings of the 2018 Conference on Empirical Methods in*  
679 *Natural Language Processing: System Demonstrations*, pp. 54–59, 2018. 3  
680

681 Christopher Torrence and Gilbert P Compo. A practical guide to wavelet analysis. *Bulletin of the*  
682 *American Meteorological society*, 79(1):61–78, 1998. 5  
683

684 Hugo Touvron, Louis Martin, Kevin Stone, Peter Albert, Amjad Almahairi, Yasmine Babaei, Niko-  
685 lay Bashlykov, Soumya Batra, Prajjwal Bhargava, Shruti Bhosale, et al. Llama 2: Open founda-  
686 tion and fine-tuned chat models. *arXiv preprint arXiv:2307.09288*, 2023. 3

687 Bryan E Usevitch. A tutorial on modern lossy wavelet image compression: foundations of jpeg  
688 2000. *IEEE signal processing magazine*, 18(5):22–35, 2001. 9  
689

690 Aaron Van Den Oord, Oriol Vinyals, et al. Neural discrete representation learning. *Advances in*  
691 *neural information processing systems*, 30, 2017. 3

692 Martin Vetterli and Jelena Kovacevic. *Wavelets and subband coding*. Prentice-hall, 1995. 5  
693

694 Gerald Woo, Chenghao Liu, Akshat Kumar, Caiming Xiong, Silvio Savarese, and Doyen Sa-  
695 hoo. Unified training of universal time series forecasting transformers. *arXiv preprint*  
696 *arXiv:2402.02592*, 2024. 3, 6, 21

697 Hao Xue and Flora D Salim. Promptcast: A new prompt-based learning paradigm for time series  
698 forecasting. *IEEE Transactions on Knowledge and Data Engineering*, 2023. 3  
699

700 Neil Zeghidour, Alejandro Luebs, Ahmed Omran, Jan Skoglund, and Marco Tagliasacchi. Sound-  
701 stream: An end-to-end neural audio codec. *IEEE/ACM Transactions on Audio, Speech, and*  
*Language Processing*, 30:495–507, 2021. 3

---

702 Xiyuan Zhang, Xiaoyong Jin, Karthick Gopalswamy, Gaurav Gupta, Youngsuk Park, Xingjian Shi,  
703 Hao Wang, Danielle C Maddix, and Yuyang Wang. First de-trend then attend: Rethinking atten-  
704 tion for time-series forecasting. *arXiv preprint arXiv:2212.08151*, 2022. 3  
705

706 Xiyuan Zhang, Ranak Roy Chowdhury, Rajesh K Gupta, and Jingbo Shang. Large language models  
707 for time series: A survey. *arXiv preprint arXiv:2402.01801*, 2024. 3  
708

709 Wenqing Zheng, SP Sharan, Ajay Kumar Jaiswal, Kevin Wang, Yihan Xi, Dejia Xu, and Zhangyang  
710 Wang. Outline, then details: Syntactically guided coarse-to-fine code generation. In *International  
711 Conference on Machine Learning*, pp. 42403–42419. PMLR, 2023. 3  
712

713 Tian Zhou, Ziqing Ma, Qingsong Wen, Xue Wang, Liang Sun, and Rong Jin. Fedformer: Frequency  
714 enhanced decomposed transformer for long-term series forecasting. In *International conference  
715 on machine learning*, pp. 27268–27286. PMLR, 2022. 3  
716

717 Zhenhai Zhu and Radu Soricut. Wavelet-based image tokenizer for vision transformers. *arXiv  
718 preprint arXiv:2405.18616*, 2024. 3  
719  
720  
721  
722  
723  
724  
725  
726  
727  
728  
729  
730  
731  
732  
733  
734  
735  
736  
737  
738  
739  
740  
741  
742  
743  
744  
745  
746  
747  
748  
749  
750  
751  
752  
753  
754  
755

756  
757  
758  
759  
760  
761  
762  
763  
764  
765  
766  
767  
768  
769  
770  
771  
772  
773  
774  
775  
776  
777  
778  
779  
780  
781  
782  
783  
784  
785  
786  
787  
788  
789  
790  
791  
792  
793  
794  
795  
796  
797  
798  
799  
800  
801  
802  
803  
804  
805  
806  
807  
808  
809

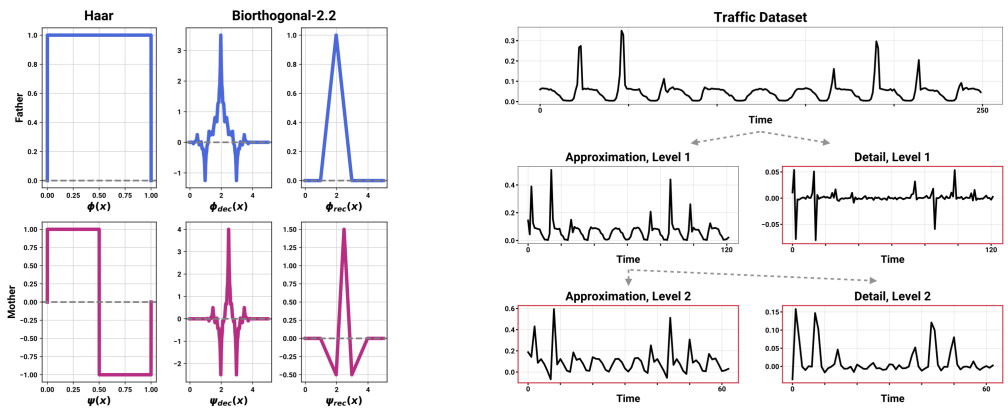


Figure 7: (Left) Mother and father wavelets for the Haar and Biorthogonal-2.2 families. Note the dual structure of the latter, which uses two filters: one for decomposition and one for reconstruction. (Right) Example of discrete wavelet transform (DWT) applied to a time series from the traffic dataset. Red boxes highlight the coefficients that are returned by the decomposition.

## A A BRIEF TOUR OF WAVELETS

### A.1 MOTIVATION: FROM THE FOURIER TRANSFORM TO THE WAVELET TRANSFORM

The Fourier Transform (FT) allows one to map a signal from the time domain to the frequency domain by computing the signal’s projection onto a basis of complex exponentials, which represent sine and cosine functions of varying frequencies. This process effectively decomposes the signal into its constituent frequency components. The main drawback of the Fourier Transform is that, while having high resolution in the frequency domain, it has zero resolution in the time domain. In other words, it cannot tell at which location in time these frequencies occur in the original signal. The Short-Time Fourier Transform (STFT) tries to overcome this issue by splitting the original signal in different windows and applying the Fourier Transform in each of them. Nonetheless, the fixed window immediately implies a trade-off: the smaller the size of the window, the higher the resolution in time domain, the lower the resolution in frequency domain, and vice versa. This is widely known as the Uncertainty Principle (Oppenheim & Schafer, 2010).

The Wavelet Transform (WT) addresses this limitation by employing a quickly decaying zero-mean oscillatory function, known as the mother wavelet, which inherently adapts its time-frequency resolution to the signal’s characteristics. By dilating or compressing the wavelet, its time support varies inversely with its frequency, thus providing high time resolution for high-frequency components and high frequency resolution for low-frequency components. This dual localization property, achieved through the modulation of the wavelet’s scale parameter, enables the WT to efficiently analyze non-stationary signals whose spectral content evolves over time, a phenomenon often referred to as *time-frequency localization* (Daubechies, 1992; Mallat, 2009).

### A.2 THE HAAR WAVELET AND THE DISCRETE WAVELET TRANSFORM

Wavelet families consist of basis functions that can be divided into two primary types: the scaling function (often referred to as the “father” wavelet), which captures the low-frequency, coarse structure of the signal (the *approximation*), and the wavelet function (often referred to as the “mother” wavelet), which captures the high-frequency components (the *detail*) of the signal. The “father” and “mother” wavelets give rise to “son” and “daughter” wavelets through scaling and translation. Here, we briefly formalize these concepts in the context of the Haar wavelet (Haar, 1911), a simple yet pedagogically significant wavelet family. For an extensive introduction to wavelets and their applications, see, for example, Mallat (2009), Daubechies (1992) and Strang & Nguyen (1996).

The Haar father wavelet is given by  $\phi(x) = \mathbb{I}(x \in [0, 1])$ . The corresponding son wavelet is

$$\phi_{k,j}(x) = 2^{j/2} \phi(2^j x - k) = \begin{cases} 2^{j/2}, & \text{if } \frac{k}{2^j} \leq x \leq \frac{k+1}{2^j} \\ 0, & \text{otherwise,} \end{cases}$$

---

**Algorithm 1** False Discovery Rate of Coefficients (FDRC)

---

- 1: For each  $d_{k,j}$ , compute two-sided p-value  $p_{k,j} = 2(1 - \Phi(|d_{k,j}|/\sigma))$  for  $H_0^{(k,j)} : d_{k,j} = 0$
  - 2: Order  $p_{k,j}$  such that  $p_{(1)} \leq \dots \leq p_m$
  - 3: Let  $i_0 = \arg \max_i p_{(i)} \leq (i/m)q$ , with  $q$  being error-rate under  $H_0$
  - 4: Let  $\lambda_{i_0} = \sigma\Phi^{-1}(1 - p_{i_0}/2)$
  - 5: Threshold all detail coefficients at level  $\lambda_{i_0}$
- 

where  $k, j \in \mathbb{N}$ . Note that  $\phi_{k,0}(x)$  generates an orthonormal basis for functions with jumps at the integers, whose space we denote by  $V_0$ . The dilations and translations  $\phi_{k,j}(x)$  span orthonormal spaces  $V_j$  for functions with jumps at  $k/2^j$ , and satisfy  $V_{j+1} \supset V_j \supset \dots \supset V_0$ . With these bases, we can represent an arbitrary function  $f(x)$  in  $V_{j+1}$  by taking a component in  $V_j$  (the *approximation*) plus the orthogonal complement of  $V_j$  to  $V_{j+1}$ , which we denote by  $W_j$  (the *detail*). In other words, we represent  $f$  in  $V_{j+1}$  by taking its orthogonal decomposition  $V_{j+1} = V_j \oplus W_j$ . The space  $W_0$  is spanned by the mother wavelet

$$\psi(x) = \phi(2x) - \phi(2x - 1) = \begin{cases} 1, & \text{if } 0 \leq x < \frac{1}{2} \\ -1, & \text{if } \frac{1}{2} \leq x \leq 1 \\ 0, & \text{otherwise} \end{cases}$$

whose dilations and translations  $\psi_{k,j} = 2^{j/2}\psi(2^j x - k)$  form an orthonormal basis for each  $W_j$ . Putting this all together, we can represent a function at different resolution levels by breaking down the level- $j$  approximation component  $V_j$  to level- $(j-1)$  detail and approximation components, and so on:  $V_J = V_J \oplus W_J = V_0 \oplus W_0 \oplus W_1 \dots \oplus W_{J-1}$ . A wavelet decomposition is then a linear combination of elements in these subspaces:

$$f(x) = \sum_{k=-\infty}^{\infty} a_k \phi_{k,J}(x) + \sum_{j=1}^J \sum_{k=-\infty}^{\infty} d_{k,j} \psi_{k,j}(x),$$

where only a finite number of coefficients  $a_k$  and  $d_{k,j}$  are non-zero.

How do we compute  $a_k$  and  $d_{k,j}$  in practice? The multi-resolution theory of [Mallat \(1989\)](#) and [Meyer \(1992\)](#) offers an elegant and efficient solution: any wavelet that generates an orthonormal basis can be characterized by a conjugate mirror filter. The mapping from a discretized signal to a sequence of wavelet coefficients is then implemented as a filter bank made of a cascade of high-pass and low-pass filters associated with the mother and father wavelets, and is called Discrete Wavelet Transform (DWT)<sup>4</sup>. For the Haar family, the approximation components are associated with averaging filters (low-pass), while the detail components are associated with distance filters (high-pass). The DWT convolves these filters with the signal and then downsamples by a factor of two to eliminate the repeated information. The result is an array of detail coefficients  $\{d_k\}_j$  and approximation coefficients  $\{a_k\}_j$ . The latter can be further decomposed into new approximation and detail coefficients at the next level and the process can continue recursively, resulting in a hierarchical and multi-resolution decomposition of the signal. [Figure 7 \(right\)](#) shows this for a particular time series.

The DWT has a computational complexity of  $\mathcal{O}(N)$ , with  $N$  being the length of the input signal. This is due to *i*) the filtering operation requiring a constant amount of work proportional to the signal length, and *ii*) the down-sampling operation halving the signal at each of the  $\log_2 N$  levels: this leads to a total amount of work equal to  $N(1 + \frac{1}{2} + \frac{1}{4} + \dots)$ , which converges to  $2N$ . Note that this is even faster than the FFT algorithm, which has a computational complexity of  $\mathcal{O}(N \log N)$ .

## B ADDITIONAL RESULTS ON DIFFERENT THRESHOLDING TECHNIQUES

[Algorithm 1](#) outlines the FDRC thresholding method step-by-step. See [Abramovich & Benjamini \(1996\)](#) for more details. During our experiments, we chose the standard  $q = 0.05$ , which corresponds to the type-I error control level of the resulting hypotheses tests.

[Figure 8](#) shows the effect of the different thresholding techniques detailed in [Section 3.2](#) on the downstream forecasting accuracy in terms of weighted quantile loss (WQL), mean absolute scaled

---

<sup>4</sup>We always refer to the *decimated* DWT. For a comparison with the *undecimated* DWT, see [Mallat \(2009\)](#).

error (MASE), and visual relative squared error (VRSE). This ablation study complements those on vocabulary size, wavelet family and decomposition level outlines in Section 4.4. Apart from the four thresholding techniques analyzed in this paper, several more exist in the literature for signal processing and image compression. We leave a comprehensive analysis of these methods and a deeper study of their effect on downstream performance to future work.

## C EVALUATION METRICS

Consider a collection of  $N$  time series  $\{\mathbf{x}_i = [x_{i,1}, \dots, x_{i,C+H}]\}_{i=1}^N$  that include both context and horizon. In Section 4, we evaluated WaveToken and all the other baselines with respect to three metrics, which we now describe more in detail: weighted quantile loss (WQL), mean absolute scaled error (MASE), and visual relative squared error (VRSE)

**Weighted quantile loss (WQL).** We use this metric to evaluate probabilistic forecasts  $q_{i,C+t}^\alpha$  — obtained by generating  $N = 20$  samples from the model for an input  $i$  — at nine quantile levels  $\alpha \in \{0.1, 0.2, 0.3, 0.4, 0.5, 0.6, 0.7, 0.8, 0.9\}$ . WQL aggregates the standard quantile loss at level  $\alpha$   $QL_\alpha(q, x)$  (Koenker & Hallock, 2001) over multiple horizon steps  $t = 1, \dots, H$  and series  $i$  by taking a weighted average:

$$\text{WQL} = 1/9 \sum_{\alpha} \frac{2 \sum_{i,t} \text{QL}_{\alpha}(q_{i,C+t}^{\alpha}, x_{i,t})}{\sum_{i,t} |x_{i,t}|},$$

where 9 is the number of quantiles used.

**Mean absolute scaled error (MASE).** We use this metric to evaluate point forecasts  $\hat{\mathbf{x}}_i = [x_{i,1}, \dots, x_{i,C+H}]$ , which we take to be the median quantile  $q_{i,C+t}^{0.5}$  across  $N = 20$  samples for probabilistic models. The MASE (Hyndman & Koehler, 2006) scales the mean absolute error by the empirical error of the seasonal naïve model:

$$\text{MASE}(\hat{\mathbf{x}}_i, \mathbf{x}_i) = \frac{C - S}{H} \frac{\sum_{t=C+1}^{C+H} |\hat{x}_{i,t} - x_{i,t}|}{\sum_{t=1}^{C-S} |x_{i,t} - x_{i,t+S}|},$$

where  $S$  is a seasonality parameter.

**Visual relative squared error (VRSE).** We use this metric to measure the frequency content of (point) forecasts relative to the ground truth. As for MASE, we take the median forecast  $q_{i,C+t}^{0.5}$  as input to the metric for probabilistic models. VRSE (Posam et al., 2024) is defined as follows:

$$\text{VRSE}(\hat{\mathbf{x}}_i, \mathbf{x}_i) = \frac{\sum_f (A_{\hat{\mathbf{x}}_i}(f) - A_{\mathbf{x}_i}(f))^2}{\sum_f (A_{\mathbf{x}_i}(f))^2},$$

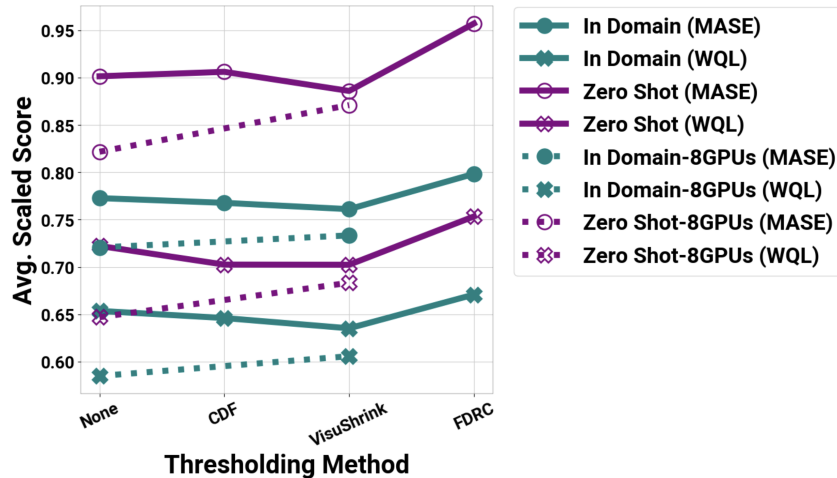


Figure 8: Effect of the different thresholding techniques of Section 3.2 on the forecasting accuracy.

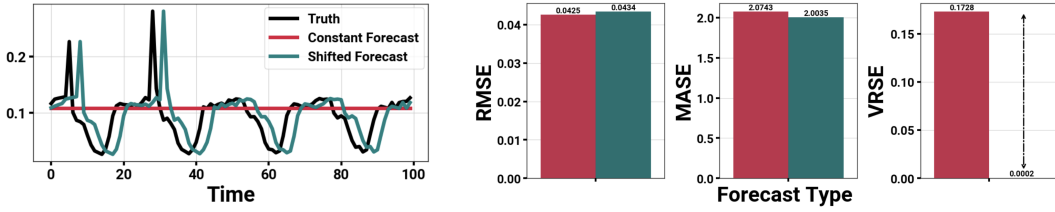


Figure 9: **Pitfall of standard evaluation metrics.** RMSE and MASE fail to distinguish a poor constant forecast from a visually much more accurate shifted forecast. By comparing the amplitudes at all frequencies, VRSE captures the difference and assigns a lower score to the shifted forecast.

where  $A_x(f)$  is the amplitude of the Fourier transform coefficient at frequency  $f$  for input  $x$ . It serves a complementary role to WQL and MASE: by computing the discrepancy between forecasts and ground truth in the amplitudes of the Fourier transform coefficients at all frequencies, this metric captures whether the forecast has the correct overall “shape”, instead of looking at it point-wise. Thus, it provides a valuable alternative in cases where other metrics clearly fail, as shown in Figure 9.

## D ADDITIONAL RESULTS: BENCHMARKS I & II

Figures 10 and 11 report the average rank across all datasets in the corresponding benchmark (in-domain and zero-shot, respectively) achieved by all the evaluated models. Tables 1-3 report the raw per-dataset values of all metrics for all models on the in-domain benchmark, along with the corresponding Aggregate Relative Score and Average Rank. Similarly, Tables 4-6 report the same values on the zero-shot benchmark. Results for WaveToken, Chronos, PatchTST, DeepAR and TFT are averaged over three seeds.

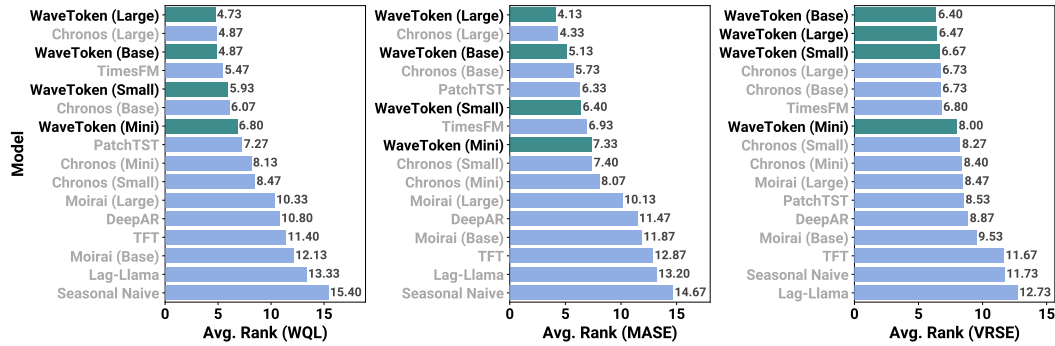


Figure 10: **WaveToken achieves best average ranks on in-domain datasets.** Average rank of models on Benchmark I (in-domain) in terms of WQL, MASE and VRSE.

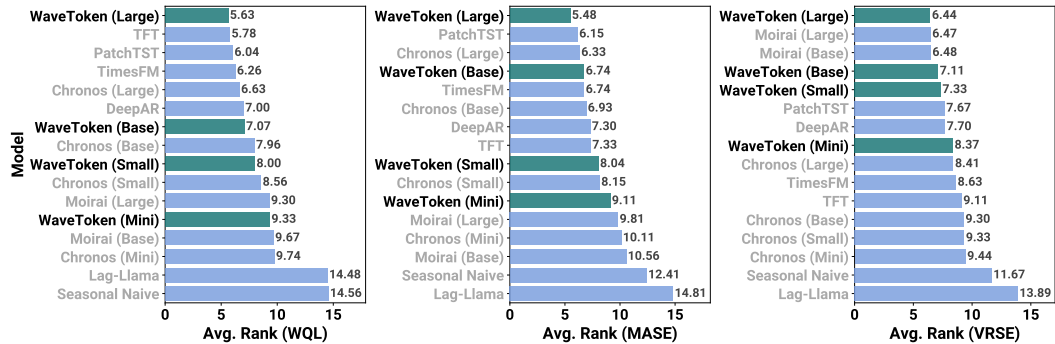


Figure 11: **WaveToken achieves best average ranks on zero-shot datasets.** Average rank of models on Benchmark II (zero-shot) in terms of WQL, MASE and VRSE.

972  
973  
974  
975  
976  
977  
978  
979  
980  
981  
982  
983  
984  
985  
986  
987  
988  
989  
990  
991  
992  
993  
994  
995  
996  
997  
998  
999  
1000  
1001  
1002  
1003  
1004  
1005  
1006  
1007  
1008  
1009  
1010  
1011  
1012  
1013  
1014  
1015  
1016  
1017  
1018  
1019  
1020  
1021  
1022  
1023  
1024  
1025

Table 1: Raw per-dataset values of WQL for all models on the in-domain benchmark.

	Pretrained Models (In Domain)							Pretrained Models (Other)				Task Specific Models			Local Models	
	Chronos (Large)	Chronos (Base)	Chronos (Small)	Chronos (Mini)	WaveToken (Mini)	WaveToken (Small)	WaveToken (Base)	WaveToken (Large)	Lstm-Llama	Mamba (Base)	Mamba (Large)	TimesFM	PatchTST	DeepAR	TFT	Seasonal Naive
Electricity (15 Min.)	<b>0.077</b>	<b>0.078</b>	0.080	0.082	0.086	0.082	0.079	0.085	0.319	0.105	0.104	0.121	0.082	0.090	0.189	0.117
Electricity (Hourly)	0.101	0.114	0.105	<b>0.089</b>	0.104	0.109	0.114	0.098	0.104	0.122	0.117	<b>0.079</b>	<b>0.089</b>	0.106	0.125	0.147
Electricity (Weekly)	<b>0.059</b>	<b>0.062</b>	0.073	0.067	0.071	0.069	0.067	0.065	0.147	0.113	0.162	<b>0.062</b>	<b>0.069</b>	0.116	0.106	0.198
KDD Cup 2018	0.272	0.268	0.289	0.271	<b>0.262</b>	<b>0.265</b>	0.270	0.282	0.369	0.287	0.277	0.288	<b>0.252</b>	0.330	0.571	0.556
London Smart Meters	0.423	0.428	0.431	0.436	0.355	0.349	<b>0.343</b>	<b>0.340</b>	0.384	0.358	0.350	0.384	<b>0.346</b>	0.405	0.365	0.541
M4 (Daily)	0.022	0.022	0.022	0.022	<b>0.021</b>	<b>0.021</b>	0.021	<b>0.021</b>	0.043	0.023	0.023	0.021	<b>0.023</b>	0.023	0.023	0.028
M4 (Hourly)	<b>0.022</b>	0.024	0.024	0.025	0.025	0.031	0.024	0.026	0.111	0.025	<b>0.022</b>	<b>0.021</b>	0.027	0.038	0.033	0.048
M4 (Monthly)	0.101	0.103	0.103	0.103	0.100	0.099	0.098	0.098	0.153	0.102	0.100	<b>0.087</b>	<b>0.095</b>	0.101	0.097	0.146
M4 (Weekly)	<b>0.037</b>	0.037	0.040	0.041	0.040	0.039	<b>0.036</b>	<b>0.036</b>	0.078	0.049	0.047	0.040	0.039	0.046	0.051	0.063
Pedestrian Counts	<b>0.187</b>	<b>0.204</b>	0.237	0.236	0.227	0.219	0.210	<b>0.195</b>	0.262	0.273	0.259	0.233	0.257	<b>0.229</b>	0.261	0.319
Rideshare	0.140	0.137	0.140	<b>0.133</b>	0.136	0.137	0.137	0.138	0.158	0.164	0.159	<b>0.133</b>	0.135	<b>0.130</b>	0.134	0.186
Taxi (30 Min.)	<b>0.268</b>	<b>0.274</b>	0.312	0.313	0.300	0.284	0.278	<b>0.267</b>	0.357	0.513	0.368	0.334	0.363	0.395	0.382	0.471
Temperature-Rain	0.663	0.669	0.685	0.704	0.651	0.646	<b>0.640</b>	<b>0.637</b>	0.717	0.655	0.685	0.646	0.646	0.804	0.718	0.670
Uber TLC (Daily)	<b>0.096</b>	<b>0.097</b>	0.100	0.105	0.112	0.107	0.103	0.102	0.176	0.115	0.108	<b>0.089</b>	0.100	0.110	0.111	0.231
Uber TLC (Hourly)	<b>0.153</b>	<b>0.153</b>	0.155	0.161	0.158	0.157	0.154	0.160	0.176	0.176	0.166	<b>0.153</b>	0.167	0.176	0.179	0.299
Agg. Relative Score	0.564	0.580	0.603	0.598	0.592	0.591	0.573	<b>0.569</b>	0.690	0.669	0.669	0.579	0.601	0.676	0.734	1.000
Avg. Rank	<b>4.867</b>	6.067	8.467	8.133	6.800	5.933	<b>4.867</b>	<b>4.733</b>	13.333	12.133	10.333	<b>5.402</b>	7.267	10.800	11.400	15.400

Table 2: Raw per-dataset values of MASE for all models on the in-domain benchmark.

	Pretrained Models (In Domain)							Pretrained Models (Other)				Task Specific Models			Local Models	
	Chronos (Large)	Chronos (Base)	Chronos (Small)	Chronos (Mini)	WaveToken (Mini)	WaveToken (Small)	WaveToken (Base)	WaveToken (Large)	Lstm-Llama	Mamba (Base)	Mamba (Large)	TimesFM	PatchTST	DeepAR	TFT	Seasonal Naive
Electricity (15 Min.)	<b>0.391</b>	<b>0.394</b>	0.418	0.445	0.443	0.422	<b>0.410</b>	0.410	1.169	0.707	0.625	0.750	0.450	0.515	1.108	0.498
Electricity (Hourly)	1.439	1.590	1.477	<b>1.348</b>	1.503	1.580	1.614	1.419	1.573	1.712	1.669	<b>1.200</b>	1.349	1.528	1.789	1.840
Electricity (Weekly)	<b>1.739</b>	1.801	1.942	1.954	1.938	1.890	1.879	1.864	2.979	2.858	2.738	<b>1.773</b>	<b>1.633</b>	2.517	2.800	3.037
KDD Cup 2018	0.683	0.646	0.687	0.667	<b>0.618</b>	<b>0.624</b>	0.631	0.654	0.844	0.661	0.656	<b>0.687</b>	<b>0.616</b>	0.779	1.022	0.994
London Smart Meters	0.828	0.838	0.846	0.857	0.771	0.759	<b>0.748</b>	<b>0.740</b>	0.792	0.770	0.754	0.822	<b>0.733</b>	0.832	0.788	0.966
M4 (Daily)	3.144	3.160	3.148	3.154	<b>3.140</b>	<b>3.145</b>	<b>3.116</b>	<b>3.116</b>	8.038	3.445	3.377	3.269	3.450	3.305	3.292	3.278
M4 (Hourly)	<b>0.682</b>	0.694	0.721	0.758	0.722	0.697	<b>0.667</b>	<b>0.671</b>	3.807	1.210	0.951	0.767	0.967	1.215	1.833	1.193
M4 (Monthly)	0.960	0.970	0.982	0.991	0.992	0.974	<b>0.956</b>	<b>0.950</b>	2.090	1.033	1.005	<b>0.886</b>	0.962	1.040	1.009	1.260
M4 (Weekly)	<b>1.928</b>	2.021	2.113	2.155	2.137	2.077	<b>2.005</b>	<b>1.948</b>	5.658	2.475	2.419	2.262	<b>1.996</b>	2.346	2.745	2.777
Pedestrian Counts	<b>0.272</b>	<b>0.286</b>	0.304	0.303	0.309	0.297	0.292	<b>0.279</b>	0.342	0.355	0.330	0.307	0.339	0.311	0.364	0.369
Rideshare	0.865	0.862	0.854	<b>0.830</b>	0.840	0.854	0.856	0.871	0.891	0.911	0.900	0.853	<b>0.827</b>	0.996	1.067	1.250
Taxi (30 Min.)	<b>0.830</b>	0.849	0.941	0.944	0.902	0.861	<b>0.848</b>	<b>0.823</b>	1.069	1.374	1.088	1.054	1.077	1.158	1.113	1.160
Temperature-Rain	0.980	0.986	1.012	1.029	0.945	0.933	<b>0.929</b>	<b>0.924</b>	1.031	0.963	0.988	1.011	1.250	1.015	0.994	2.243
Uber TLC (Daily)	0.821	0.839	0.870	0.906	0.952	0.938	0.887	0.876	1.289	0.937	0.874	<b>0.803</b>	<b>0.813</b>	0.905	0.916	1.378
Uber TLC (Hourly)	<b>0.670</b>	<b>0.673</b>	0.677	0.689	0.786	0.777	0.771	0.779	0.711	0.728	0.716	0.677	0.696	0.703	0.746	0.931
Agg. Relative Score	<b>0.695</b>	0.706	0.727	0.732	0.729	0.718	0.708	<b>0.698</b>	1.141	0.856	0.806	0.745	0.740	0.821	0.939	1.000
Avg. Rank	<b>4.333</b>	5.733	7.400	8.067	7.333	6.400	<b>5.133</b>	<b>4.133</b>	13.200	11.867	10.133	6.933	6.333	11.467	12.867	14.667

Table 3: Raw per-dataset values of VRSE for all models on the in-domain benchmark.

	Pretrained Models (In Domain)							Pretrained Models (Other)				Task Specific Models			Local Models	
	Chronos (Large)	Chronos (Base)	Chronos (Small)	Chronos (Mini)	WaveToken (Mini)	WaveToken (Small)	WaveToken (Base)	WaveToken (Large)	Lstm-Llama	Mamba (Base)	Mamba (Large)	TimesFM	PatchTST	DeepAR	TFT	Seasonal Naive
Electricity (15 Min.)	0.022	0.023	<b>0.021</b>	0.024	0.027	0.026	0.024	0.027	1.354	<b>0.018</b>	0.024	0.033	0.022	0.030	0.109	0.032
Electricity (Hourly)	0.012	0.013	0.012	0.009	0.013	0.010	0.012	0.013	<b>0.008</b>	0.014	0.012	0.01	<b>0.007</b>	<b>0.008</b>	0.010	0.011
Electricity (Weekly)	0.015	<b>0.014</b>	0.022	0.021	0.021	0.019	0.016	<b>0.014</b>	0.099	0.093	0.179	<b>0.011</b>	0.026	0.070	0.057	0.159
KDD Cup 2018	<b>0.099</b>	<b>0.101</b>	<b>0.108</b>	0.115	0.113	0.118	0.123	0.131	0.157	0.129	0.119	0.151	0.117	0.131	0.996	0.284
London Smart Meters	0.323	0.337	0.341	0.352	0.213	0.213	0.208	<b>0.205</b>	0.252	0.208	<b>0.188</b>	0.274	0.241	0.309	0.261	<b>0.177</b>
M4 (Daily)	0.010	0.007	0.005	0.007	0.004	<b>0.004</b>	0.004	<b>0.004</b>	0.022	0.005	0.004	<b>0.004</b>	0.005	0.006	0.007	0.007
M4 (Hourly)	0.000	0.000	0.001	0.000	0.000	0.001	0.001	0.001	0.003	<b>0.000</b>	<b>0.000</b>	<b>0.000</b>	0.001	0.001	0.001	0.002
M4 (Monthly)	0.047	0.047	0.048	0.047	0.045	0.044	0.044	0.043	0.080	0.042	<b>0.042</b>	<b>0.040</b>	0.043	<b>0.041</b>	0.044	0.048
M4 (Weekly)	<b>0.003</b>	0.003	0.004	0.004	0.004	0.004	<b>0.003</b>	<b>0.003</b>	0.020	0.006	0.005	0.004	0.004	0.005	0.008	0.008
Pedestrian Counts	<b>0.083</b>	0.104	0.110	0.108	0.111	0.109	0.105	<b>0.099</b>	0.121	0.126	0.133	0.111	0.128	<b>0.088</b>	0.099	0.118
Rideshare	0.043	0.041	0.043	<b>0.041</b>	0.043	0.043	0.044	0.043	0.052	0.066	0.064	0.049	0.041	<b>0.031</b>	0.049	<b>0.032</b>
Taxi (30 Min.)	<b>0.027</b>	0.099	0.136	0.126	0.118	0.104	<b>0.087</b>	<b>0.087</b>	0.169	0.329	0.156	0.172	0.214	0.208	0.222	0.108
Temperature-Rain	0.596	0.633	0.677	0.712	0.512	0.505	<b>0.419</b>	<b>0.409</b>	0.423	<b>0.419</b>	0.538	0.584	0.584	0.537	0.542	1.715
Uber TLC (Daily)	0.024	0.023	<b>0.023</b>	0.024	0.028	<b>0.023</b>	0.024	0.024	0.067	0.031	0.024	<b>0.024</b>	0.023	0.024	0.031	0.115
Uber TLC (Hourly)	0.020	<b>0.019</b>	<b>0.020</b>	0.024	0.022	<b>0.021</b>	<b>0.020</b>	0.024	0.047	0.029	0.023	0.030	0.030	0.030	0.028	0.058
Agg. Relative Score	0.550	0.547	0.582	0.591	0.555	0.567	<b>0.540</b>	<b>0.540</b>	1.350	0.684	0.664	0.548	0.608	0.681	0.921	1.000
Avg. Rank	6.733	6.733	8.267	8.400	8.000	6.667	<b>6.400</b>	<b>6.400</b>	12.733	9.533	8.467	6.800	8.533	8.867	11.667	11.733

## E ADDITIONAL RESULTS: LONG-HORIZON FORECASTING

Figure 12 shows results on a long-horizon benchmark constructed by increasing the forecast length  $H$  of each dataset in Benchmark II (Zero-Shot) by a factor of 2 and 3, implying maximum horizons of 112 and 168 (for NN5 Daily). Benchmark I (In-Domain) was not used as increasing the forecast length over the prescribed ones (see Table 9) would imply mixing the test and training portions of the datasets. The datasets in Benchmark II without sufficient history in all time series to allow for longer horizons have been skipped. WaveToken-Base outperforms other foundation models across all three metrics in the  $H \times 2$  setting. When  $H \times 3$ , TimesFM performs better with respect to WQL only. All results for Chronos and WaveToken are averaged across three different seeds.

## F ADDITIONAL RESULTS: QUALITATIVE ANALYSIS

Figures 13, 14 and 15 show all the cross-attention maps for the 12 decoder layers of Chronos-Base (left) and WaveToken-Base (right) when forecasting the spiky data of the second row in Figure 1.

1026  
1027  
1028  
1029  
1030  
1031  
1032  
1033  
1034  
1035  
1036  
1037  
1038  
1039  
1040  
1041  
1042  
1043  
1044  
1045  
1046  
1047  
1048  
1049  
1050  
1051  
1052  
1053  
1054  
1055  
1056  
1057  
1058  
1059  
1060  
1061  
1062  
1063  
1064  
1065  
1066  
1067  
1068  
1069  
1070  
1071  
1072  
1073  
1074  
1075  
1076  
1077  
1078  
1079

Table 4: Raw per-dataset values of WQL for all models on the zero-shot benchmark.

	Pretrained Models (Zero Shot)								Pretrained Models (Other)				Task Specific Models			Local Models
	Chinese (Large)	Chinese (Base)	Chinese (Small)	Chinese (Mini)	WowTokan (Mini)	WowTokan (Small)	WowTokan (Base)	WowTokan (Large)	Lang-Jama	Mamba (Base)	Mamba (Large)	TimeRM	PatchTST	DeepAR	TFT	Seasonal Noise
Australian Electricity	0.067	0.075	0.074	0.063	0.094	0.065	0.075	0.071	0.097	0.055	0.046	0.089	0.057	0.087	0.036	0.084
Car Parts	1.060	1.087	1.029	1.024	0.923	0.986	0.994	1.001	1.011	1.654	1.621	1.019	0.998	0.967	0.871	1.600
CIFF 2016	0.014	0.013	0.015	0.013	0.014	0.012	0.014	0.012	0.041	0.011	0.031	0.020	0.140	0.156	0.011	0.015
Covid Deaths	0.045	0.048	0.059	0.084	0.057	0.050	0.048	0.049	0.276	0.038	0.035	0.204	0.065	0.108	0.034	0.133
Dominick	0.332	0.332	0.338	0.346	0.352	0.348	0.343	0.342	0.443	0.361	0.346	0.426	0.345	0.364	0.320	0.453
ERCOT Load	0.019	0.016	0.018	0.018	0.017	0.015	0.015	0.019	0.033	0.019	0.021	0.021	0.017	0.032	0.037	0.037
ETT (15 Min.)	0.068	0.069	0.064	0.072	0.068	0.071	0.063	0.061	0.080	0.075	0.070	0.084	0.054	0.069	0.075	0.141
ETT (Hourly)	0.073	0.081	0.080	0.085	0.080	0.072	0.073	0.074	0.106	0.095	0.084	0.092	0.071	0.081	0.082	0.122
Exchange Rate	0.015	0.014	0.015	0.012	0.015	0.014	0.013	0.011	0.010	0.012	0.013	0.010	0.009	0.011	0.013	0.013
FRED-MD	0.020	0.022	0.017	0.017	0.026	0.022	0.027	0.026	0.389	0.047	0.048	0.035	0.042	0.043	0.112	0.122
Hospital	0.056	0.056	0.057	0.058	0.060	0.059	0.057	0.055	0.093	0.060	0.057	0.051	0.070	0.056	0.053	0.073
M1 (Monthly)	0.130	0.128	0.139	0.138	0.140	0.139	0.134	0.128	0.196	0.155	0.151	0.123	0.165	0.150	0.175	0.191
M1 (Quarterly)	0.107	0.105	0.103	0.103	0.111	0.110	0.111	0.119	0.141	0.108	0.107	0.087	0.078	0.089	0.122	0.150
M1 (Yearly)	0.183	0.181	0.172	0.179	0.177	0.173	0.167	0.166	0.293	0.195	0.199	0.163	0.165	0.139	0.124	0.209
M3 (Monthly)	0.096	0.097	0.100	0.099	0.099	0.098	0.097	0.095	0.155	0.102	0.101	0.093	0.113	0.099	0.096	0.149
M3 (Quarterly)	0.074	0.076	0.079	0.080	0.079	0.077	0.076	0.075	0.134	0.080	0.085	0.072	0.074	0.073	0.071	0.101
M3 (Yearly)	0.151	0.153	0.155	0.159	0.140	0.149	0.151	0.143	0.192	0.166	0.170	0.123	0.133	0.130	0.130	0.167
M4 (Quarterly)	0.082	0.083	0.084	0.086	0.081	0.081	0.080	0.079	0.132	0.081	0.080	0.074	0.074	0.080	0.080	0.119
M4 (Yearly)	0.134	0.137	0.136	0.140	0.134	0.136	0.134	0.130	0.178	0.121	0.138	0.117	0.106	0.111	0.110	0.161
M5	0.587	0.586	0.590	0.602	0.592	0.593	0.590	0.590	0.625	0.592	0.584	0.559	0.567	0.567	0.560	0.604
NNS (Daily)	0.156	0.161	0.169	0.173	0.190	0.176	0.162	0.161	0.261	0.181	0.162	0.160	0.149	0.155	0.145	0.425
NNS (Weekly)	0.091	0.091	0.090	0.091	0.094	0.092	0.092	0.090	0.111	0.092	0.092	0.086	0.081	0.087	0.086	0.123
Tourism (Monthly)	0.100	0.103	0.113	0.109	0.117	0.103	0.096	0.093	0.213	0.123	0.113	0.088	0.092	0.092	0.096	0.104
Tourism (Quarterly)	0.061	0.069	0.069	0.074	0.071	0.070	0.066	0.063	0.202	0.100	0.085	0.069	0.074	0.072	0.074	0.119
Tourism (Yearly)	0.183	0.207	0.200	0.218	0.184	0.197	0.193	0.192	0.238	0.167	0.163	0.148	0.137	0.127	0.102	0.209
Traffic	0.256	0.264	0.263	0.264	0.240	0.250	0.260	0.250	0.256	0.225	0.231	0.184	0.246	0.233	0.264	0.362
Weather	0.139	0.140	0.143	0.150	0.142	0.140	0.139	0.137	0.164	0.135	0.132	0.150	0.143	0.147	0.151	0.217
Agg. Relative Score	0.645	0.662	0.667	0.678	0.683	0.655	0.655	0.644	1.097	0.698	0.707	0.692	0.684	0.733	0.639	1.000
Avg. Rank	6.630	7.963	8.556	9.741	9.333	8.000	7.074	5.630	14.481	8.660	9.296	6.629	6.037	7.500	5.778	14.556

Table 5: Raw per-dataset values of MASE for all models on the zero-shot benchmark.

	Pretrained Models (Zero Shot)								Pretrained Models (Other)				Task Specific Models			Local Models
	Chinese (Large)	Chinese (Base)	Chinese (Small)	Chinese (Mini)	WowTokan (Mini)	WowTokan (Small)	WowTokan (Base)	WowTokan (Large)	Lang-Jama	Mamba (Base)	Mamba (Large)	TimeRM	PatchTST	DeepAR	TFT	Seasonal Noise
Australian Electricity	1.333	1.319	1.399	1.114	1.657	1.287	1.404	1.310	1.635	1.250	0.995	1.631	0.871	1.473	0.810	1.253
Car Parts	0.906	0.899	0.887	0.891	0.847	0.860	0.865	0.873	0.816	1.734	1.540	0.893	0.803	0.798	0.799	1.201
CIFF 2016	0.986	0.981	0.989	1.051	1.066	1.012	0.997	0.977	2.235	1.208	1.138	0.928	1.537	1.533	1.533	1.289
Covid Deaths	42.550	42.687	42.670	43.621	38.051	37.939	37.670	36.909	78.456	33.062	33.062	36.627	36.465	38.203	30.835	46.912
Dominick	0.818	0.816	0.819	0.833	0.825	0.823	0.821	0.822	1.250	0.880	0.845	1.220	0.867	0.851	0.800	0.871
ERCOT Load	0.617	0.550	0.573	0.588	0.565	0.510	0.519	0.627	0.834	0.590	0.600	0.590	0.553	0.553	0.553	0.761
ETT (15 Min.)	0.741	0.739	0.710	0.792	0.729	0.710	0.724	0.642	0.967	0.968	0.765	1.037	0.652	0.874	0.962	1.169
ETT (Hourly)	0.735	0.789	0.789	0.795	0.757	0.723	0.726	0.726	1.002	0.895	0.839	0.890	0.729	0.814	0.875	0.952
Exchange Rate	2.375	2.433	2.252	2.030	2.306	2.268	2.224	2.348	3.087	1.536	1.293	3.310	1.540	1.615	2.361	1.740
FRED-MD	0.500	0.486	0.496	0.483	0.510	0.503	0.501	0.500	2.283	0.609	0.598	0.484	0.745	0.621	0.929	1.101
Hospital	0.810	0.810	0.815	0.817	0.713	0.709	0.697	0.697	0.939	0.821	0.824	0.759	0.859	0.804	0.799	0.921
M1 (Monthly)	4.301	4.624	4.659	4.958	4.737	4.895	4.751	4.449	7.149	4.629	4.707	4.004	4.042	3.085	4.316	4.894
M1 (Quarterly)	0.857	0.868	0.855	0.900	0.912	0.888	0.871	0.858	1.846	0.947	0.924	0.870	1.255	0.943	0.916	1.146
M1 (Yearly)	1.181	1.199	1.256	1.289	1.272	1.247	1.223	1.216	2.886	1.433	1.439	1.150	1.264	1.209	1.160	1.425
M3 (Monthly)	3.106	3.209	3.276	3.385	3.079	3.142	3.185	2.992	5.114	3.654	3.823	2.697	2.949	2.827	2.820	3.172
M3 (Quarterly)	1.216	1.231	1.246	1.271	1.243	1.226	1.212	1.210	2.663	1.285	1.259	1.160	1.150	1.254	1.248	1.602
M3 (Yearly)	3.606	3.678	3.651	3.743	3.688	3.731	3.652	3.550	5.866	3.601	4.174	3.339	3.072	3.178	3.119	3.974
M4 (Yearly)	0.944	0.939	0.940	0.944	0.944	0.945	0.941	0.940	0.965	1.440	0.930	0.912	0.912	0.956	0.909	1.399
NNS (Daily)	0.573	0.585	0.615	0.642	0.732	0.678	0.621	0.615	0.992	0.700	0.626	0.629	0.575	0.585	0.556	1.292
NNS (Weekly)	0.940	0.938	0.944	0.945	0.966	0.951	0.948	0.948	1.141	0.991	0.994	0.949	0.867	0.867	0.866	1.063
Tourism (Monthly)	1.761	1.828	1.900	1.950	1.997	1.821	1.695	1.633	3.030	2.040	1.911	1.541	1.572	1.529	1.686	1.631
Tourism (Quarterly)	1.677	1.717	1.730	1.829	1.836	1.804	1.762	1.725	3.695	2.712	2.306	1.731	1.723	1.886	1.729	1.690
Tourism (Yearly)	3.755	3.900	3.901	4.048	3.635	3.852	3.699	3.689	5.755	3.060	3.284	3.234	3.138	3.702	3.047	3.552
Traffic	0.804	0.808	0.837	0.859	0.875	0.877	0.843	0.829	0.817	0.843	0.838	0.790	0.732	0.732	0.890	1.119
Weather	0.822	0.824	0.836	0.853	0.846	0.834	0.830	0.822	1.001	0.831	0.808	0.912	0.860	0.911	0.913	1.004
Agg. Relative Score	0.823	0.832	0.841	0.850	0.848	0.828	0.817	0.810	1.291	0.908	0.875	0.846	0.810	0.843	0.847	1.000
Avg. Rank	6.333	6.926	8.148	10.111	9.111	8.037	6.741	5.481	14.815	10.556	9.815	6.741	6.148	7.296	7.333	12.407

Table 6: Raw per-dataset values of VRSE for all models on the zero-shot benchmark.

	Pretrained Models (Zero Shot)								Pretrained Models (Other)				Task Specific Models			Local Models
	Chinese (Large)	Chinese (Base)	Chinese (Small)	Chinese (Mini)	WowTokan (Mini)	WowTokan (Small)	WowTokan (Base)	WowTokan (Large)	Lang-Jama	Mamba (Base)	Mamba (Large)	TimeRM	PatchTST	DeepAR	TFT	Seasonal Noise
Australian Electricity	0.008	0.008	0.008	0.010	0.012	0.005	0.009	0.010	0.006	0.004	0.005	0.013	0.002	0.012	0.001	0.008
Car Parts	0.906	0.922	0.867	0.843	0.863	0.854	0.845	0.848	0.933	0.967	0.946	0.993	0.976	0.908	0.948	0.827
CIFF 2016	0.000	0.000	0.000	0.000	0.000	0.000	0.000	0.000	0.000	0.005	0.000	0.000	0.001	0.035	0.030	0.000
Covid Deaths	0.003	0.004	0.006	0.012	0.006	0.005	0.003	0.003	0.079	0.003	0.009	0.099	0.011	0.045	0.002	0.026
Dominick	0.273	0.279	0.290	0.308	0.242	0.243	0.241	0.245	0.283	0.244	0.242	0.278	0.279	0.271	0.311	0.401
ERCOT Load	0.001	0.001	0.001	0.001	0.001	0.000	0.001	0.001	0.004	0.001	0.001	0.001	0.001	0.003	0.001	0.002
ETT (15 Min.)	0.006	0.006	0.006	0.008	0.007	0.006	0.006	0.005	0.034	0.007	0.006	0.010	0.004	0.006	0.006	0.019
ETT (Hourly)	0.007	0.007	0.008	0.009	0.007	0.006	0.006	0.007	0.02							

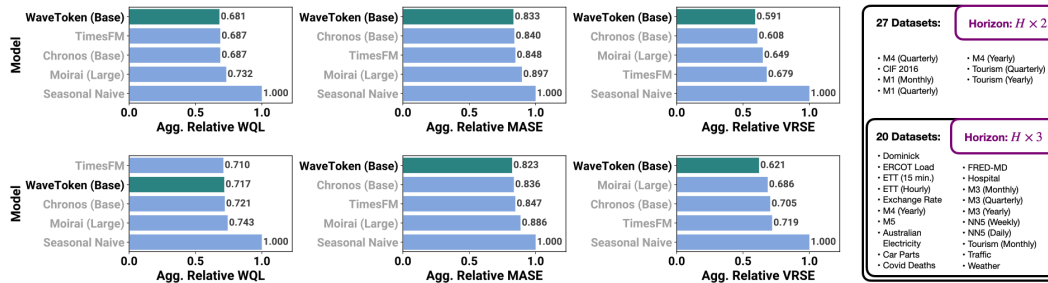


Figure 12: Long-horizon benchmark constructed by increasing the forecast length of each dataset in Benchmark II (Zero-Shot) by a factor of 2 and 3. (Top row) Results with horizon multiplied by 2: WaveToken-Base outperforms other foundation models across all three metrics. (Bottom row) Results with horizon multiplied by 3: WaveToken-Base outperforms other foundation models with respect to MASE and VRSE. TimesFM performs better with respect to WQL. (Right) List of all datasets included in the two long-horizons benchmarks. All results for Chronos and WaveToken are averaged across three different seeds.

## G DATASETS AND BASELINES

In this section we report details on all the datasets (Tables 7 and 9) and baselines (Table 8) used for the experiments of Section 4. For the SeasonalNaive baseline, we relied on the implementation available in the StatsForecast library (Garza et al., 2022). For the task-specific deep learning models, we used their implementations available in the GluonTS library (Alexandrov et al., 2020). Finally, we used the corresponding reference implementations for Lag-llama<sup>5</sup> (Rasul et al., 2023), Moirai<sup>6</sup> (Woo et al., 2024), TimesFM<sup>7</sup> (Das et al., 2023) and Chronos<sup>8</sup> (Ansari et al., 2024).

Table 7: Breakdown of the datasets and baselines used for training and evaluation.

Data Subset	# Datasets	# Series	Usage	Evaluation Baselines
Pretraining-only	13	795,936	pretraining	-
Benchmark I	15	97,272	pretraining and in-domain evaluation	SeasonalNaive, DeepAR, TFT, PatchTST Lag-Llama, Moirai-1.0-R (Base & Large), Chronos (Mini-Large), TimesFM
Benchmark II	27	190,674	zero-shot evaluation	All of the above

Table 8: Baseline models and hyper-parameter choices. Hyper-parameters not specified are set to defaults in their respective implementations.  $C$  stands for context length,  $d_h$  for hidden layer dimension,  $n_L$  for number of layers, and  $n_H$  for number of heads.

Model	Model Type	Implementation	Probabilistic	Hyperparameters
SeasonalNaive	Local	StatsForecast	Yes	N/A
DeepAR	Task-specific	GluonTS	Yes	$d_h = 40, n_L = 2$
TFT	Task-specific	GluonTS	Yes	$d_h = 32, n_H = 4$
PatchTST	Task-specific	GluonTS	Yes	Patch length: 16, Stride: 8, $d_h = 32, n_L = 2, n_H = 4$
Lag-Llama	Pretrained	Reference	Yes	$C = 32$
Moirai-1.0-R	Pretrained	Reference	Yes	$C = 1024$ , Patch length: selected by dataset-specific validation
TimesFM	Pretrained	Reference	Yes	All hyperparameters set to defaults from the released models
Chronos	Pretrained	Reference	Yes	All hyperparameters set to defaults from the released models
WaveToken	Pretrained	Reference	Yes	All hyperparameters set to defaults as in Chronos

<sup>5</sup><https://github.com/time-series-foundation-models/lag-llama>

<sup>6</sup><https://github.com/SalesforceAIRResearch/uni2ts>

<sup>7</sup><https://github.com/google-research/timesfm>

<sup>8</sup><https://github.com/amazon-science/chronos-forecasting>

1134  
 1135  
 1136  
 1137  
 1138  
 1139  
 1140  
 1141  
 1142  
 1143  
 1144  
 1145  
 1146  
 1147  
 1148  
 1149  
 1150  
 1151  
 1152  
 1153  
 1154  
 1155  
 1156  
 1157  
 1158  
 1159  
 1160  
 1161  
 1162  
 1163  
 1164  
 1165  
 1166  
 1167  
 1168  
 1169  
 1170  
 1171  
 1172  
 1173  
 1174  
 1175  
 1176  
 1177  
 1178  
 1179  
 1180  
 1181  
 1182  
 1183  
 1184  
 1185  
 1186  
 1187

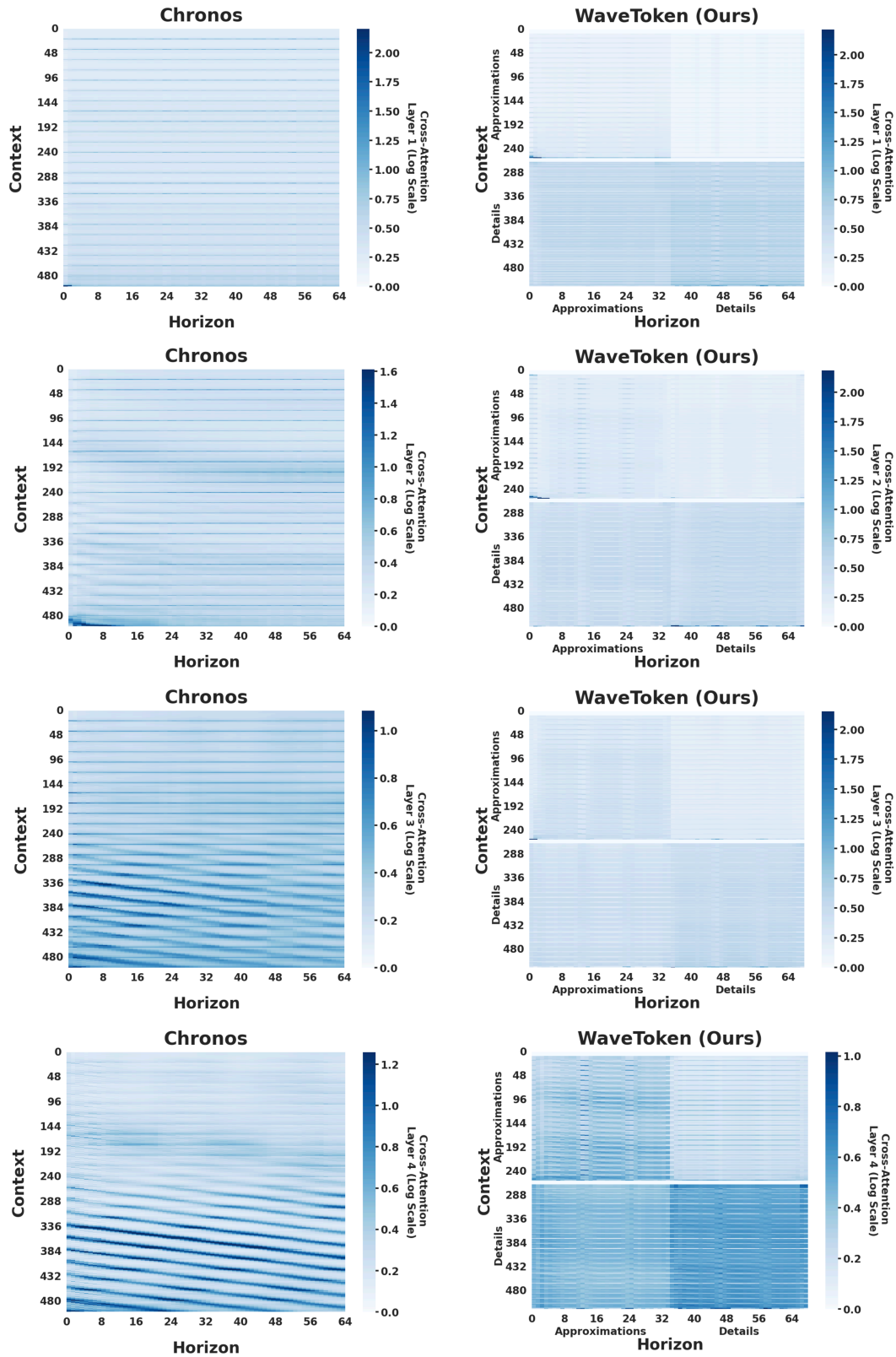


Figure 13: Cross-attention maps for the first to fourth (from top) decoder layers of Chronos-Base (left) and WaveToken-Base (right) when forecasting the spiky data of the second row in Figure 1.

1188  
 1189  
 1190  
 1191  
 1192  
 1193  
 1194  
 1195  
 1196  
 1197  
 1198  
 1199  
 1200  
 1201  
 1202  
 1203  
 1204  
 1205  
 1206  
 1207  
 1208  
 1209  
 1210  
 1211  
 1212  
 1213  
 1214  
 1215  
 1216  
 1217  
 1218  
 1219  
 1220  
 1221  
 1222  
 1223  
 1224  
 1225  
 1226  
 1227  
 1228  
 1229  
 1230  
 1231  
 1232  
 1233  
 1234  
 1235  
 1236  
 1237  
 1238  
 1239  
 1240  
 1241

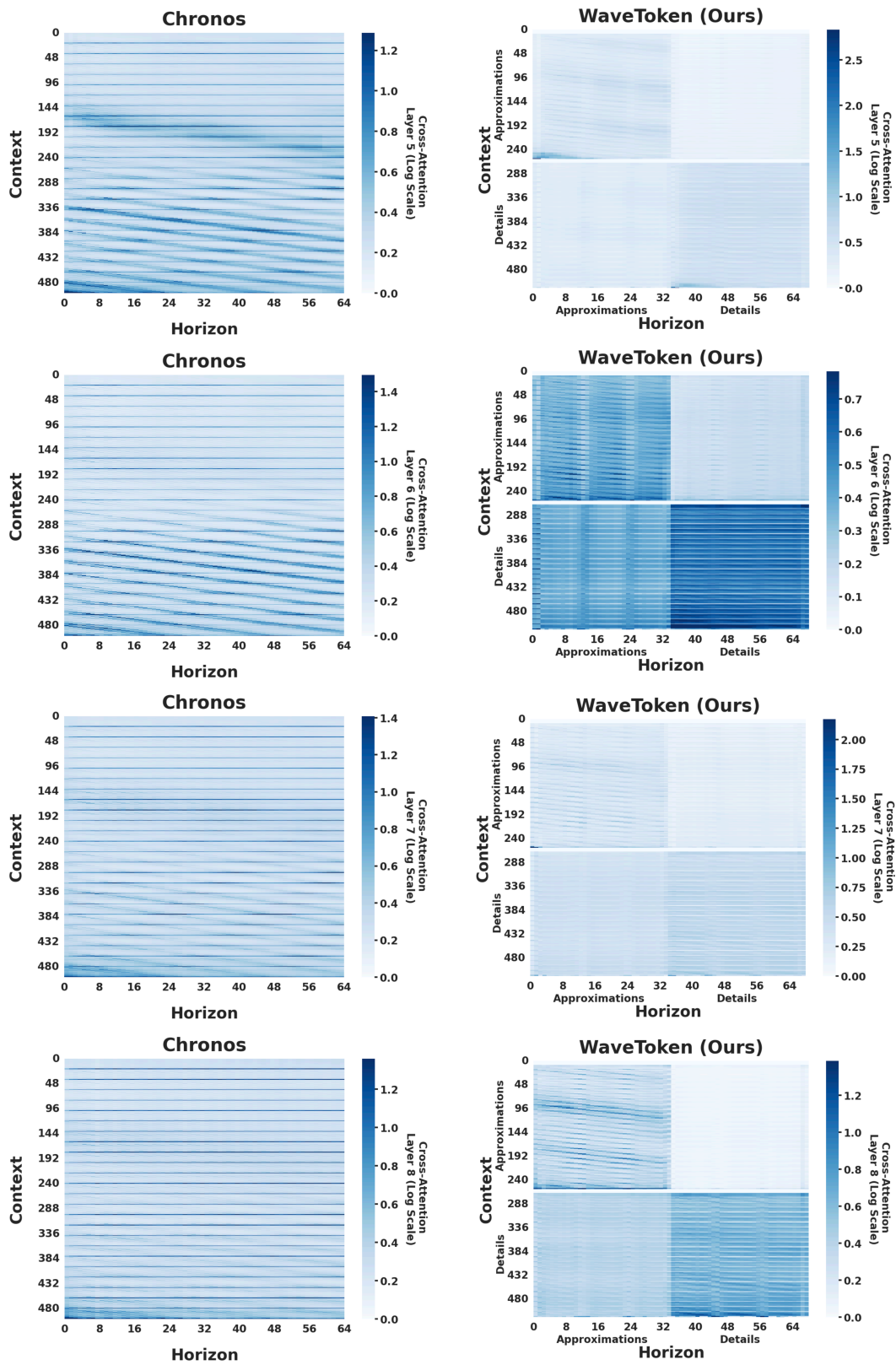


Figure 14: Cross-attention maps for the fifth to eighth (from top) decoder layers of Chronos-Base (left) and WaveToken-Base (right) when forecasting the spiky data of the second row in Figure 1.

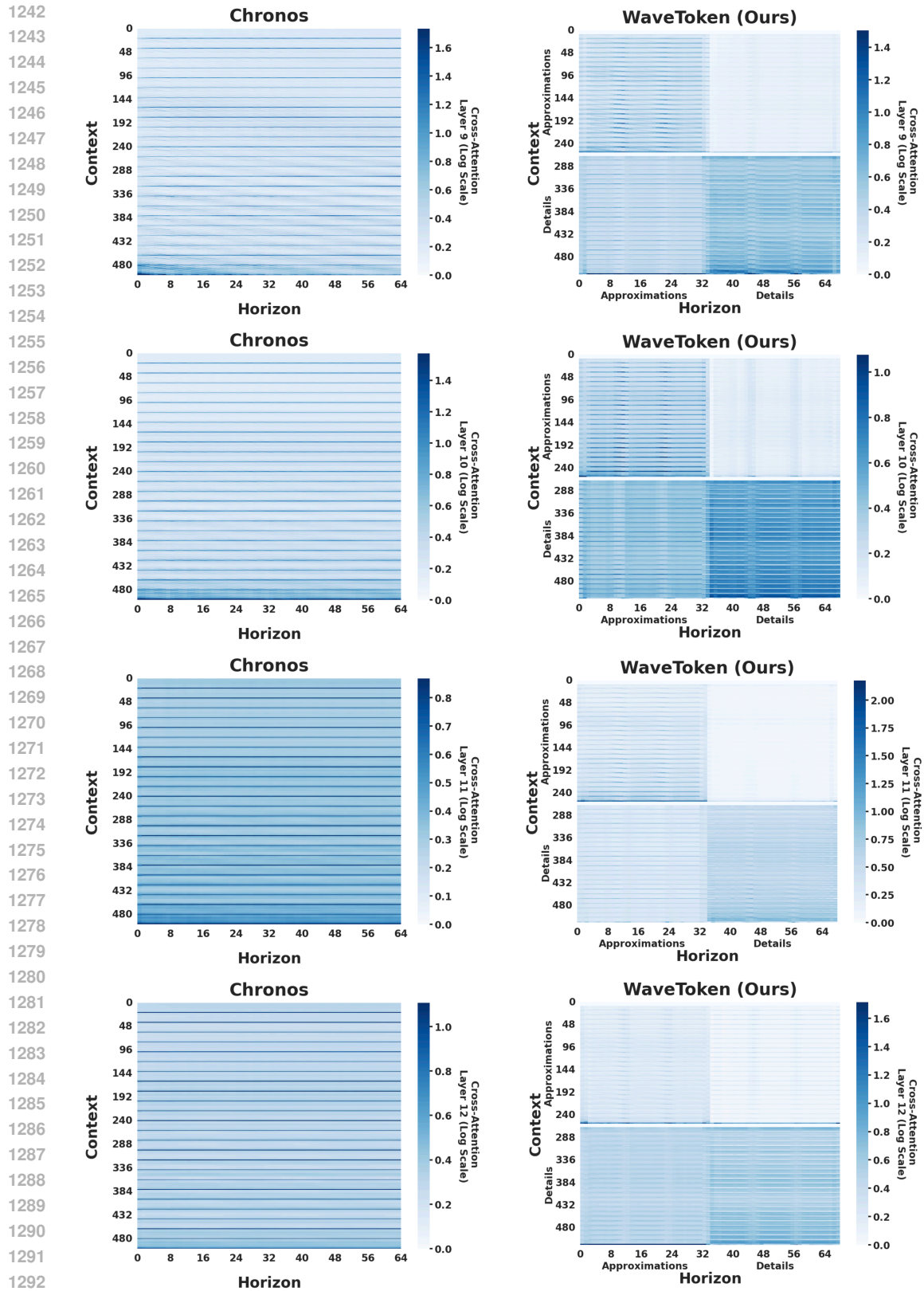


Figure 15: Cross-attention maps for the ninth to twelfth (from top) decoder layers of Chronos-Base (left) and WaveToken-Base (right) when forecasting the spiky data of the second row in Figure 1.

1296  
1297  
1298  
1299  
1300  
1301  
1302  
1303  
1304  
1305  
1306  
1307  
1308  
1309  
1310  
1311  
1312  
1313  
1314  
1315  
1316  
1317  
1318  
1319  
1320  
1321  
1322  
1323  
1324  
1325  
1326  
1327  
1328  
1329  
1330  
1331  
1332  
1333  
1334  
1335  
1336  
1337  
1338  
1339  
1340  
1341  
1342  
1343  
1344  
1345  
1346  
1347  
1348  
1349

Table 9: Details of all datasets used for experiments, as collected by Ansari et al. (2024), partitioned according to how they are used for training and evaluation of WaveToken models.

Dataset	Domain	Freq.	Num. Series	Series Length			Prediction Length ( $H$ )
				min	avg	max	
<b>Pretraining-only</b>							
Solar (5 Min.)	energy	5min	5166	105120	105120	105120	-
Solar (Hourly)	energy	1h	5166	8760	8760	8760	-
Spanish Energy and Weather	energy	1h	66	35064	35064	35064	-
Taxi (Hourly)	transport	1h	2428	734	739	744	-
USHCN	nature	1D	6090	5906	38653	59283	-
Weatherbench (Daily)	nature	1D	225280	14609	14609	14610	-
Weatherbench (Hourly)	nature	1h	225280	350633	350639	350640	-
Weatherbench (Weekly)	nature	1W	225280	2087	2087	2087	-
Wiki Daily (100k)	web	1D	100000	2741	2741	2741	-
Wind Farms (Daily)	energy	1D	337	71	354	366	-
Wind Farms (Hourly)	energy	1h	337	1715	8514	8784	-
<b>In-domain evaluation</b>							
Electricity (15 Min.)	energy	15min	370	16032	113341	140256	24
Electricity (Hourly)	energy	1h	321	26304	26304	26304	24
Electricity (Weekly)	energy	1W	321	156	156	156	8
KDD Cup 2018	nature	1h	270	9504	10897	10920	48
London Smart Meters	energy	30min	5560	288	29951	39648	48
M4 (Daily)	various	1D	4227	107	2371	9933	14
M4 (Hourly)	various	1h	414	748	901	1008	48
M4 (Monthly)	various	1M	48000	60	234	2812	18
M4 (Weekly)	various	1W	359	93	1035	2610	13
Pedestrian Counts	transport	1h	66	576	47459	96424	48
Rideshare	transport	1h	2340	541	541	541	24
Taxi (30 Min.)	transport	30min	2428	1469	1478	1488	48
Temperature-Rain	nature	1D	32072	725	725	725	30
Uber TLC (Daily)	transport	1D	262	181	181	181	7
Uber TLC (Hourly)	transport	1h	262	4344	4344	4344	24
<b>Zero-shot evaluation</b>							
Australian Electricity	energy	30min	5	230736	231052	232272	48
CIF 2016	banking	1M	72	28	98	120	12
Car Parts	retail	1M	2674	51	51	51	12
Covid Deaths	healthcare	1D	266	212	212	212	30
Dominick	retail	1D	100014	201	296	399	8
ERCOT Load	energy	1h	8	154854	154854	154854	24
ETT (15 Min.)	energy	15min	14	69680	69680	69680	24
ETT (Hourly)	energy	1h	14	17420	17420	17420	24
Exchange Rate	finance	1B	8	7588	7588	7588	30
FRED-MD	economic	1M	107	728	728	728	12
Hospital	healthcare	1M	767	84	84	84	12
M1 (Monthly)	various	1M	617	48	90	150	18
M1 (Quarterly)	various	3M	203	18	48	114	8
M1 (Yearly)	various	1Y	181	15	24	58	6
M3 (Monthly)	various	1M	1428	66	117	144	18
M3 (Quarterly)	various	3M	756	24	48	72	8
M3 (Yearly)	various	1Y	645	20	28	47	6
M4 (Quarterly)	various	3M	24000	24	100	874	8
M4 (Yearly)	various	1Y	23000	19	37	841	6
M5	retail	1D	30490	124	1562	1969	28
NN5 (Daily)	finance	1D	111	791	791	791	56
NN5 (Weekly)	finance	1W	111	113	113	113	8
Tourism (Monthly)	various	1M	366	91	298	333	24
Tourism (Quarterly)	various	1Q	427	30	99	130	8
Tourism (Yearly)	various	1Y	518	11	24	47	4
Traffic	transport	1h	862	17544	17544	17544	24
Weather	nature	1D	3010	1332	14296	65981	30